PHILOSOPHICAL TRANSACTIONS OF THE ROYAL SOCIETY A MATHEMATICAL, PHYSICAL & ENGINEERING SCIENCES

Nonlinear Effects on Shoaling Surface Gravity Waves

M. H. Freilich and R. T. Guza

Phil. Trans. R. Soc. Lond. A 1984 **311**, 1-41
doi: 10.1098/rsta.1984.0019

Phil. Trans. R. Soc. Lond. A **311**, 1–41 (1984) [1]
Printed in Great Britain

NONLINEAR EFFECTS ON SHOALING SURFACE GRAVITY WAVES

BY M. H. FREILICH* AND R. T. GUZA
Center for Coastal Studies, Scripps Institution of Oceanography, La Jolla, California 92093, *U.S.A.*

(*Communicated by G. B. Whitham, F.R.S. – Received* 17 *March* 1983)

CONTENTS

Two nonlinear models that describe the shoaling of unidirectional surface gravity waves are developed. Based on variants of Boussinesq's equations, the models are cast as a set of coupled evolution equations for the amplitudes and phases of the temporal Fourier modes of the wave field. Triad interactions across the entire wind–wave frequency band (0.05–0.25 Hz) provide the mechanism for cross spectral energy transfers and modal phase modifications as the waves propagate shoreward through the shoaling region (10–3 m depth).

A field experiment, designed to test the operational validity of the nonlinear shoaling models, provided data on wave parameters over a wide range of conditions. Three representative data sets illustrating different initial spectral shapes and subsequent evolutions are compared with predictions of the nonlinear shoaling models and linear, finite-depth theory.

Power spectral comparisons, as well as spectra of coherence and relative phase between model predictions and data, indicate that the nonlinear models accurately

* Present address: Jet Propulsion Laboratory, California Institute of Technology, Pasadena, Ca 91109, U.S.A.

predict Fourier coefficients of the wave field through the shoaling region for all data sets. Differences between the predictions of the various models are related to differences in the models' dispersion relations. Although generally inferior to the nonlinear models, linear, finite-depth theory accurately predicts Fourier coefficients in regions of physical and frequency space where nonlinear evolution of the power spectrum is not observed, thus verifying the validity of the linear, finite-depth dispersion relation in limited portions of physical and frequency space in the shoaling region.

1. Introduction

As surface gravity waves approach a beach their shapes change dramatically until, in most cases, they break. The aim of the work reported here is to develop and test in the field a model that describes the transformations that occur as a spectrum of surface gravity waves propagates shoreward over a mildly sloping bottom. Although wave breaking and subsequent surf zone fluid motions are both visually spectacular and scientifically important for such processes as sediment transport, the present work will concentrate on the 'shoaling region', defined here to be the area between approximately 10 and 3 m depth, outside and specifically excluding the break zone. This shoaling region has a horizontal extent of approximately 300 m at the southern California experimental site. In order to be applicable to most field situations, any shoaling model must allow for a complicated wave field characterized by a broad, arbitrarily shaped frequency spectrum. Some areas, owing to local beach orientation with respect to the larger scale coastline or offshore topographic features, require a realistic shoaling model to accommodate waves incident at a relatively high angle to the bottom contours at the outer edge of the shoaling region. The models discussed here allow broad frequency spectra but are restricted to waves almost normally incident to a beach with straight, parallel contours, a simplification appropriate for the experimental site.

Linear theory has often been used as the basis for shoaling wave models. Assuming that the nonlinear terms in the finite-depth, inviscid, irrotational equations of motion and boundary conditions are small, several authors (Hanson 1926; Friederichs 1948; Stoker 1957; for a review see Whitham 1979) have found exact solutions for the case where beach slope h_x is given by $h_x = M\pi/2N$, M and N integers. For the physically interesting case of small bottom slope, approximate (W.K.B.) solutions have been obtained on the assumption of no reflected energy. These solutions locally satisfy flat-bottom equations; slow changes in wave amplitude and phase due to varying depth are obtained by satisfying solubility conditions at the next order in an expansion in bottom slope (Chu & Mei 1970). The amplitude changes predicted by the W.K.B. solutions are of course equal to those obtained by applying conservation of lowest order energy flux to the lowest order equations (Rayleigh 1911).

Owing to the linear nature of the approximate governing equations used in the above models, solutions for motions with differing frequencies can be combined to satisfy arbitrary conditions at a given on–offshore point. Slowly varying, linear, finite-depth theory is roughly consistent (to the 20% level) with observations of r.m.s. shoaling wave heights, but some spectral features are apparently due to nonlinear effects (Guza & Thornton 1980). It seems intuitively clear that the processes immediately preceding wave breaking are essentially nonlinear. As there are well known techniques for incorporating at least weak nonlinearity into a physical problem, attention has naturally turned toward the nonlinear aspects of wave shoaling.

Considerable effort has been expended in attempts to use Stokes-type perturbation expan-

sions on the full, finite-depth equations of motion and boundary conditions for waves propagating over a sloping bottom (Skjelbreia & Hendrickson 1960; LeMehaute & Webb 1964; Chu & Mei 1970). Most authors expand the dependent variables in a small parameter equivalent to the Ursell number $a\lambda^2/h^3$ (where a is a typical sea-surface elevation, λ a horizontal length scale, and h a typical depth), while Chu & Mei expand in both Ursell number and bottom slope. Temporally periodic solutions composed of the primary wave and its forced harmonics are found, locally equivalent to the classic Stokes (1847) solution for the case of a flat bottom. Although the double expansion of Chu & Mei is an exception, bottom slope is generally considered to be of a higher order than that to which the expansions are carried; W.K.B. 'energy flux' arguments are applied as in the linear theory, and results are found in which varying depth leads to spatially varying amplitudes of the primary and harmonics. In order for the solutions to remain consistent, the forced harmonics cannot grow to be larger than, or even comparable with, the fundamental. Solutions are steady in the sense that the amplitudes of the fundamental and its harmonics would not change in the absence of the sloping bottom.

The necessity of the Ursell number remaining small in order to justify low-order truncation of the series expansion is a particularly stringent restriction for long waves characteristic of those found in the shoaling region. The applicability of slowly varying Stokes theory as a realistic model of wave shoaling is thus suspect. Fortunately, shallow water approximations to the equations of motion can be derived and have been found to be exceptionally tractable. In the limit of very long waves, the classic shallow water equations (Airy 1845; Stoker 1957) can be used. Carrier & Greenspan (1958) found an exact solution to these equations for the purely reflective problem of non-breaking waves on a sloping beach. However, Ursell (1953) had demonstrated that just as the near-linear Stokes-type perturbation solutions were valid only for $a\lambda^2/h^3 \ll 1$, so the classic shallow water equations were valid only for $a\lambda^2/h^3 \gg 1$. Parameters typical of wind waves in the shoaling region lead to Ursell numbers that are $O(1)$.

Boussinesq (1871) derived a set of evolution equations that contained terms accounting for weak dispersion due to finite depth, and weak nonlinearity due to finite amplitude. Korteweg & deVries (1895) followed with a single equation (the K. de V. equation) describing a similar system supporting unidirectional wave motion only. These two sets of equations are valid in the régime where the Ursell number is $O(1)$. Boussinesq and Korteweg & deVries obtained exact solutions of their respective equations that described waves of permanent form propagating in water of constant depth. Considerable effort in the last two decades has been devoted to exploring the limits and applicability of the Boussinesq and K. de V. equations, which not only admit exact solutions, but also appear to model quantitatively many aspects of long wave propagation in laboratory tanks. Starting with Peregrine's (1967) derivation of Boussinesq's equations for mild bottom slope, many authors have conducted extensive experimental and numerical studies of the development and eventual fate of solitary and cnoidal waves propagating over varying bottom topography (see Miles's 1980 review). Stiassnie & Peregrine (1980) and Flick *et al.* (1981) partly match Stokes-type predictions to those of solitary–cnoidal wave theories to describe the shoaling of monochromatic waves from deep water to shallow depths near the break zone. James (1974) similarly matched Stokes waves to 'hyperbolic waves' (more tractable approximations to cnoidal waves). However, because of the rather restricted initial and boundary conditions required for the exact solutions of Boussinesq- or K. de V.-type equations, it is not clear that detailed studies of these solutions will lead to general shoaling models for surface gravity waves.

PHILOSOPHICAL TRANSACTIONS OF THE ROYAL SOCIETY A MATHEMATICAL, PHYSICAL & ENGINEERING SCIENCES

Field observations occasionally show incoming wave energy to be concentrated in a narrow band of frequencies and directions. In such cases, the basically monochromatic assumptions about the nature of the wave field inherent in Stokes and solitary–cnoidal wave shoaling theories are not *prima facie* violated. However, wave spectra measured at the seaward edge of the shoaling region are often broad, or contain multiple peaks (not harmonics). Following the suggestion of Phillips (1960) that energy could be transferred between deep water gravity waves of different frequencies and directions, Hasselmann (1962, 1963, 1966) developed a model for nonlinear resonant transfers in a general, continuous spectrum of deep water waves. Much additional work followed on this essentially statistical problem (Benney & Saffman 1966; Newell 1968; Willebrand 1975; Longuet-Higgins 1976; Herterich & Hasselmann 1980). Such work has demonstrated that the quartet resonance mechanism can indeed cause significant changes in the spectrum of the wave field over distances of several hundred kilometres or more. Importantly, although details of the evolution depend on the spectrum, the models themselves do not require a specific initial spectral shape.

Armstrong *et al.* (1962) and Bretherton (1964) introduced the concept of 'near resonance' in weakly nonlinear systems with discrete spectra. They showed that, on moderate length or time scales, significant cross-spectral energy transfers and modal phase modifications could take place if the resonance conditions were only approximately satisfied. Mei & Unluata (1972) and Bryant (1973) demonstrated that Boussinesq-type equations for long waves propagating over a flat bottom support near resonant interactions at second (quadratic) order. Because the near resonance in the long wave solutions occurs at lower order than does the exact (cubic) resonance for deep water gravity waves, significant energy transfers and phase modifications can take place in several hundred meters in shallow water rather than the many kilometres necessary in deep water.

In §2 of this work two nonlinear models for the evolution of the wave field in the shoaling region are developed, based on sloping bottom Boussinesq-type equations. The mechanism for the shoaling transformation is seen to be nonlinear triad interactions across the entire wind wave frequency band. The models predict both cross-spectral energy transfers and nonlinear modal phase changes. In §3 a field experiment is described in which detailed measurements of wave parameters were collected throughout the shoaling region. Measurements are compared with model predictions for a variety of wave conditions in §4, and further discussion and conclusions appear in §5.

2. Theory

In this section we derive equations for the evolution of the amplitudes and phases of inviscid, irrotational, wind waves propagating shoreward over slowly varying, impermeable topography. The rate equations are a consequence of near resonant triad interactions allowed by the governing, Boussinesq-type master equations.

To justify the use of shallow water equations, periodic solutions are first found for the special case of linear waves over a flat bottom of arbitrary depth. The dispersion relation obtained indicates that for motions in the wind wave frequency band defined here as 0.05–0.25 Hz, wavelengths are large compared with the water depth almost everywhere in the shoaling region. This motivates the use of a simplified set of nonlinear equations of motion valid only for such long waves. Small-amplitude solutions of these equations yield a dispersion relation which is at most mildly dispersive. We show that such a system supports weakly nonlinear triad inter-

actions, resulting in slow variations of the amplitudes and the phases of lowest order solutions. Two-scale methods are used to solve the nonlinear, long wave equations; at lowest order, the linear, flat bottom dispersion relation is obtained as well as a relation between sea–surface elevation and velocity potential. Carrying the solution to next order yields equations for the on–offshore evolution of lowest order amplitudes and phases.

(*a*) *The equations of motion*

The equations of motion and boundary conditions for the one-dimensional, irrotational motion of an inviscid, incompressible fluid over an impermeable bottom are well known:

$$\nabla^2\phi = 0, \quad -h(x) \leqslant z \leqslant \eta(x,t), \tag{1a}$$

$$\phi_z = -h_x\phi_x, \quad z = -h(x), \tag{1b}$$

$$\eta_t + (\eta_x\phi_x) - \phi_z = 0, \quad z = \eta(x,t), \tag{1c}$$

$$g\eta + \phi_t + \tfrac{1}{2}(\phi_x^2 + \phi_z^2) = 0, \quad z = \eta(x,t), \tag{1d}$$

where $\nabla^2 = \partial^2/\partial x^2 + \partial^2/\partial z^2$, $-h(x)$ is the bottom, $\eta(x,t)$ is the free surface, and $\phi(x,z,t)$ is the velocity potential. (See figure 1 for a definitional sketch.) It is possible (Stokes 1847) to

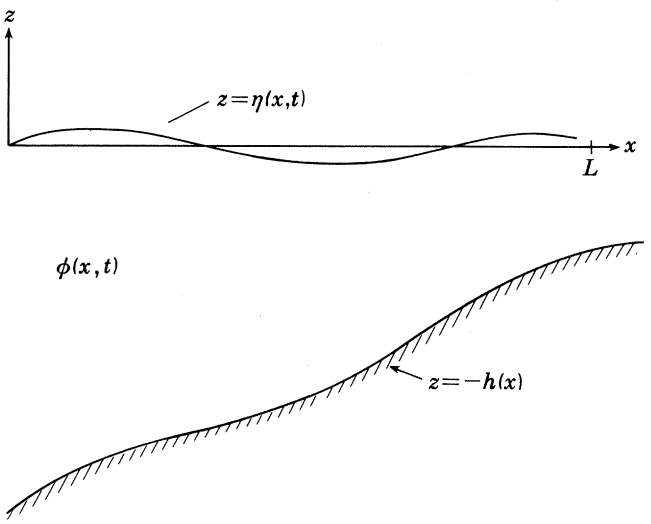

FIGURE 1. Definitional sketch and coordinate system.

nondimensionalize, expand, and scale the system (1) such that the nonlinear terms in the surface boundary conditions (1*c*) and (1*d*) differ from the other terms by the factor a_0/λ_0, where a_0 is a typical sea–surface elevation and λ_0 a horizontal scale of motion. If a_0/λ_0 and the bottom slope h_x are small, then a solution of the lowest order equations is

$$\eta = a\cos(kx - \sigma t), \tag{2a}$$

$$\phi = \frac{ga\cosh k(z+h)}{\sigma\cosh(kh)}\sin(kx - \sigma t), \tag{2b}$$

$$\sigma^2 = gk\tanh(kh). \tag{2c}$$

Evaluation of the dispersion relation (2*c*) shows that in 10 m depth (at the outer edge of the experimental shoaling region), even short wind waves of period 4 s have a wavelength greater

than twice the water depth. Ursell (1953) pointed out that for waves long compared with the depth, the common Stokes-type expansion and linearization leading to (2) is valid only when $a_0\lambda_0^2/h_0^3 \ll 1$ (where h_0 is a typical depth). It is clear that the requirement that the Ursell number, $a_0\lambda_0^2/h_0^3$, remain small will invalidate the solutions (2) in shallow water except for the smallest amplitude wind waves.

This severe constraint on wave amplitudes can be relaxed if it is assumed *a priori* that the depth is small. The derivations of equations for finite-amplitude long waves were originally given by Boussinesq (1871) and Korteweg & deVries (1895), and later put on firmer formal ground by Friederichs (1948) and Keller (1948). The formal derivations begin by non-dimensionalizing and scaling the horizontal and vertical coordinates in (1) differently. The dependent variables are then expanded in a power series in $(h_0/\lambda_0)^2$ and (a_0/h_0). Boussinesq's equations are obtained by retaining terms up to first order in each of these parameters, thus modelling the effects of both weak dispersion and weak nonlinearity. These equations admit exact solutions corresponding to waves of permanent form, the so-called cnoidal and solitary waves. Generalizations of Boussinesq's and the K. de V. equations to include the effects of sloping bottoms were obtained by Mei & LeMehaute (1966), Peregrine (1967), Ostrovskiy & Pelinovskiy (1970), Grimshaw (1970), and Johnson (1973). Svendsen & Hansen (1978) discuss the bottom slope magnitudes for which the equations can be expected to remain valid models of the physical system from which they were derived. Although the solitary and cnoidal wave literature is extensive, to our knowledge no analytical or numerical work has been done pertaining to the transformation, on a sloping bottom, of temporally periodic waveforms of arbitrary spectral shape.

Boussinesq's equations for waves over a mildly sloping bottom have been derived by Peregrine (1967) and Grimshaw (1970). In dimensional coordinates, the equations can be written

$$g\eta_x + \overline{\phi}_{xt} + \tfrac{1}{2}(\overline{\phi}_x^2)_x = \tfrac{1}{2}(\overline{\phi}_{xt}h)_{xx} - \tfrac{1}{6}h^2\overline{\phi}_{xxxt}, \tag{3a}$$

$$\eta_t + (h\overline{\phi}_x)_x + (\eta\overline{\phi}_x)_x = 0, \tag{3b}$$

where $\overline{\phi}$ is depth-averaged velocity potential. As there are no explicit restrictions on the applicability of (3) as equations for wind waves in the shoaling region, a few comments are warranted. First, equations (3) are good approximations to (1) only for the case of long waves of moderate nonlinearity

$$O((h_0/\lambda_0)^2) \sim O(a_0/h_0) \ll 1.$$

Even if the above conditions on the parameters of the solution are valid, the equations cannot be considered a valid model for all values of the independent variables; terms of formal order $(h_0/\lambda_0)^4$, $(a_0/h_0)^2$, etc., which were neglected in the derivation of (3) may have $O(1)$ effects on the solution over nondimensional times and distances $O((h_0/\lambda_0)^{-4}, (a_0/h_0)^{-2})$. Additionally, the neglected terms can be viewed as adding errors of their order into any local solution. Exact solutions of the approximate equations cannot be expected to be exact solutions of the full equations of motion obeyed by a real system, nor are they exact solutions of the approximate but more complete equations (1). It is thus wholly consistent with the derivation of approximate equations to pursue approximate solutions (which have a more obviously limited validity) in an attempt to model specific phenomena. This is true even when, as in the present case, exact solutions of the approximate equations can be obtained for a limited class of initial and boundary conditions.

PHILOSOPHICAL TRANSACTIONS OF THE ROYAL SOCIETY A MATHEMATICAL, PHYSICAL & ENGINEERING SCIENCES

(*b*) *A consistent shoaling model*

The equations (3) can be recast as a set of approximate equations describing the spatial evolution of Fourier modes of the wave field. The resulting equations are valid for a wave field that is everywhere periodic in time in a region of extent large compared to a typical wavelength, but no larger than the *a priori* limits on the validity of (3) discussed above. In the following, the implicit assumption $(h_0/\lambda_0)^2 \sim (a_0/h_0)$ used in the derivation of (3) is made explicit upon re-scaling by the substitution $\beta = \rho\alpha$ (where $\rho = O(1)$ is the inverse of the Ursell number and α, β represent the order of nonlinear and dispersive terms, respectively). Mild and slowly varying bottom slope is made explicit by the assumption $h = h(\alpha x)$; then $\mathrm{d}^n h/\mathrm{d}x^n = O(\alpha^n)$. The equations in non-dimensional form then become

$$\eta_x + \overline{\phi}_{xt} - \tfrac{1}{3}\rho\alpha h^2 \overline{\phi}_{xxxt} + \tfrac{1}{2}\alpha(\overline{\phi}_x^2)_x = 0, \quad \eta_t + (\overline{\phi}_x h)_x + \alpha(\eta\overline{\phi}_x)_x = 0. \tag{4a, b}$$

Before embarking on the protracted algebra required for a perturbation-type solution, it is instructive to investigate the lowest order form of (4) obtained by setting $\alpha = 0$:

$$\overline{\phi}_t + \eta = 0; \quad \eta_t + h\overline{\phi}_{xx} = 0. \tag{5a, b}$$

This set is just the linear shallow water equations for constant depth (Stoker 1957). Periodic solutions of (5) of the form

$$\eta = a\cos(kx - \sigma t + \Lambda), \quad \overline{\phi} = Q\sin(kx - \sigma t + \Lambda), \tag{6a, b}$$

yield the relations

$$Q = a/\sigma, \quad k = \sigma/h^{\frac{1}{2}}. \tag{7a, b}$$

The linear dependence of k on σ in the dispersion relation (7*b*) reflects the well known fact that linear waves in extremely shallow water are non-dispersive, with all frequencies propagating at a uniform phase speed that depends only on the (non-dimensional) depth. It must be emphasized, however, that the governing equations (4) explicitly contain terms representing weak dispersion $(-\tfrac{1}{3}\rho\alpha h^2\overline{\phi}_{xxxt})$ as well as weak nonlinearity $(\tfrac{1}{2}\alpha(\overline{\phi}_x^2)_x, \alpha(\eta\overline{\phi}_x)_x)$. These terms appear at next order, and there arises the possibility of either nonlinearly generated forced waves or resonant triads.

Second order forced waves are caused by nonlinear interactions among lowest order free waves resulting in time and space periodicities that are incommensurate with the lowest order dispersion relation. Forced wave amplitudes are constrained to be always small, of $O(\alpha)$.

Nonlinear forcing of lowest order free modes results if the conditions

$$\pm\sigma_1 \pm \sigma_2 - \sigma_3 = 0, \quad \pm\boldsymbol{k}_1 \pm \boldsymbol{k}_2 - \boldsymbol{k}_3 = 0, \tag{8a, b}$$

are satisfied, where each $(\sigma_n, \boldsymbol{k}_n)$ pair satisfies the lowest order dispersion relation. Clearly, if motion is unidirectional and the lowest order waves are not dispersive, (8*a*) and (8*b*) are not independent constraints. This is the case for the dispersion relation (7*b*), and thus nonlinear triad interactions governed by (4) must occur between all modes. The salient features of these resonant triad interactions are:

(i) $O(1)$ energy can be slowly (on length scales large compared with wavelengths) transferred between interacting modes;

(ii) similarly and simultaneously, slow phase shifts (equivalent to small changes in the phase speeds) can occur among interacting modes. The scales on which significant nonlinear energy or phase changes can occur is $O(\alpha^{-1})$, where α is the (small) measure of the size of the

nonlinear terms (Bretherton 1964; Phillips 1977). Bretherton (1964) and Armstrong *et al.* (1962) used methods similar to the two-scale technique of Krylov & Bogoliubov (see Minorsky 1974 or Cole 1968) to obtain asymptotic solutions that describe isolated resonant triads. In the following, similar techniques will be employed to derive approximate solutions of (4).

We expand the dependent variables $\overline{\phi}$, η in a power series in α:

$$\overline{\phi} = \overline{\phi}_1 + \alpha\overline{\phi}_2 + \ldots, \quad \eta = \eta_1 + \alpha\eta_2 + \ldots. \tag{9a, b}$$

The solution will be carried only as far as the first term in each expansion. Anticipating nonlinear triad interactions, we shall allow parameters of the solutions $\overline{\phi}_1$, η_1 to vary slowly with x. Specifically, we assume solutions of the form

$$\overline{\phi}_1 = \sum_n Q_n(x) \sin(\Psi_n(x) - \sigma_n t), \quad \eta_1 = \sum_n a_n(x) \cos(\Psi_n(x) - \sigma_n t), \tag{10a, b}$$

where $\sigma_n = n\Delta\sigma$, and Q_n, a_n are functions of the slow space variable $\xi = \alpha x$ (similar to $h = h(\alpha x)$) such that

$$\frac{\mathrm{d}^i}{\mathrm{d}x^i}\begin{bmatrix} a_n \\ Q_n \end{bmatrix} = \alpha^i \frac{\mathrm{d}^i}{\mathrm{d}\xi^i}\begin{bmatrix} a_n \\ Q_n \end{bmatrix} + O(\alpha^{i+1}). \tag{11}$$

The spatial phase function $\Psi_n(x)$ has both $O(1)$ derivatives (corresponding to the basic wave motion itself) and higher order derivatives (slow phase changes arising from both the sloping bottom and the anticipated effects of nonlinear interactions):

$$\frac{\mathrm{d}}{\mathrm{d}x}\Psi_n(x) = k_n(\xi) + \alpha T_n(\xi) + O(\alpha^2), \tag{12a}$$

$$\frac{\mathrm{d}^2}{\mathrm{d}x^2}\Psi_n(x) = \alpha\frac{\mathrm{d}}{\mathrm{d}\xi}k_n(\xi) + O(\alpha^2). \tag{12b}$$

When (10)–(12) are substituted into (4), the lowest order relations (7) are obtained. Higher-order solutions are more compactly pursued if (7*a*) and (7*b*) are cross-differentiated and subtracted to eliminate linear terms containing η:

$$\overline{\phi}_{1xtt} - h\overline{\phi}_{1xxx} - \tfrac{1}{3}\rho\alpha h^2\overline{\phi}_{1xxxtt} + \tfrac{1}{2}\alpha(\overline{\phi}_{1x}^2)_{xt} - 2\alpha h_\xi\overline{\phi}_{1xx} - \alpha(\eta\overline{\phi}_{1x})_{xx} = 0. \tag{13}$$

Substitution of (10)–(12) into (13) yields, at $O(\alpha)$,

$$\begin{aligned}\sum_n \{Q_{n\xi}(3hk_n^2 - \sigma_n^2) + Q_n k_n(3hk_{n\xi} + 2h_\xi k_n)\} \sin\theta_n + \sum_n \{Q_n T_n(3hk_n^2 - \sigma_n^2) - \tfrac{1}{3}\rho h^2 Q_n k_n^3\sigma_n^2\} \cos\theta_n \\ + \tfrac{1}{2}\sum_j\sum_m Q_j Q_m k_m(k_j + k_m)\{\tfrac{1}{2}k_j(\sigma_j + \sigma_m) + \sigma_j(k_j + k_m)\} \cos(\theta_j + \theta_m) \\ + \tfrac{1}{2}\sum_j\sum_m Q_j Q_m k_m(k_j - k_m)\{\tfrac{1}{2}k_j(\sigma_j - \sigma_m) + \sigma_j(k_j - k_m)\} \cos(\theta_j - \theta_m) = \Omega(\overline{\phi}_2),\end{aligned} \tag{14}$$

where $\theta_q = (\Psi_q - \sigma_q t)$ and Ω is the linear operator

$$\Omega = (\partial^3/\partial x\,\partial t^2 - h\,\partial^3/\partial x^3).$$

If all waves are unidirectional, then (7*b*) can be used to eliminate k. The technique of Krylov & Bogoliubov, essentially a solubility constraint, requires that $\overline{\phi}_2$ does not contain time periodicities common to $\overline{\phi}_1$. Since the sums in (14) are taken over all (positive) frequencies, $\overline{\phi}_2$ can thus be set identically equal to zero. Then, applying the condition (8*a*), assuming unidirec-

tionality, and making use of the fact that all frequencies are harmonics of a small frequency $\Delta\sigma$, we obtain

$$\sum_n \{2Q_{n\xi}\sigma_n^2 + Q_n(\tfrac{1}{2}\sigma_n^2 h_\xi/h)\}\sin\theta_n + \sum_n Q_n\sigma_n^2\{2T_n - \tfrac{1}{3}\rho h^{\frac{1}{2}}\sigma_n^3\}\cos\theta_n$$
$$= -\tfrac{3}{4}h^{-\frac{3}{2}}\sum_j\sum_m Q_j Q_{(n-j)}\sigma_j\sigma_{(n-j)}\sigma_n^2\sin(\theta_j+\theta_{(n-j)})$$
$$-\tfrac{3}{4}h^{-\frac{3}{2}}\sum_j\sum_m Q_j Q_{(j-n)}\sigma_j\sigma_{(j-n)}\sigma_n^2\sin(\theta_j-\theta_{(j-n)}). \qquad (15)$$

Expanding the arguments $\theta_j \pm \theta_{\pm(n-j)}$, adding and subtracting Ψ_n, and equating like frequencies, we obtain two evolution equations for each mode:

$$Q_{n\xi} = -\tfrac{1}{4}Q_n\frac{h_\xi}{h} + \tfrac{3}{8}h^{-\frac{3}{2}}\sum_j\{Q_j Q_{(n-j)}\sigma_j\sigma_{(n-j)}\sin(\Psi_j+\Psi_{(n-j)}-\Psi_n)$$
$$+ Q_j Q_{(j-n)}\sigma_j\sigma_{(j-n)}\sin(\Psi_j-\Psi_{(j-n)}-\Psi_n)$$
$$+ Q_j Q_{(j+n)}\sigma_j\sigma_{(j+n)}\sin(\Psi_{(j+n)}-\Psi_j-\Psi_n)\}; \qquad (16a)$$

$$T_n = \tfrac{1}{6}\rho h^{\frac{1}{2}}\sigma_n^3 - \frac{3}{8Q_n}h^{-\frac{3}{2}}\sum_j\{Q_j Q_{(n-j)}\sigma_j\sigma_{(n-j)}\sin(\Psi_j+\Psi_{(n-j)}-\Psi_n)$$
$$+ Q_j Q_{(j-n)}\sigma_j\sigma_{(j-n)}\sin(\Psi_j-\Psi_{(j-n)}-\Psi_n)$$
$$+ Q_j Q_{(j+n)}\sigma_j\sigma_{(j+n)}\sin(\Psi_{(j+n)}-\Psi_j-\Psi_n)\}. \qquad (16b)$$

The problem is thus reduced to solving the system (16) (hereafter referred to as the c.s.m. (consistent shoaling model)) of coupled, first order, ordinary differential equations for modal amplitudes and phases.

If it is assumed that all energy in the shoaling region is propagating shoreward (thus neglecting reflection in the shoaling region), knowledge of the Fourier coefficients of sea–surface elevation and velocity potential at a single on–offshore location provides a sufficient boundary condition for the solution of the evolution equations. Boundary conditions of the form

$$\bar{\phi}_1(0,t) = \sum_n Q'_n\cos(\Lambda_n+\sigma_n t), \qquad (17a)$$

$$\eta_1(0,t) = \sum_n a'_n\cos(\Lambda_n+\sigma_n t), \qquad (17c)$$

$$\sigma_n = n\Delta\sigma, \qquad (17c)$$

can be used to set the integration constants $Q_n(0)$, $\Psi_n(0)$. The solution $\bar{\phi} = \bar{\phi}_1 + O(\alpha^2)$ is a first-order solution uniformly valid over a horizontal extent $O(\alpha^{-1})$. For larger horizontal distances, the cumulative effects of the neglected derivative terms

$$\frac{\mathrm{d}^n}{\mathrm{d}x^n}\begin{bmatrix}Q_j\\T_j\end{bmatrix}, \quad n \geqslant 2,$$

are expected to invalidate the solution. Furthermore, terms of this formal order have been omitted from the basic equations (3) so that higher-order solutions are pointless unless higher-order versions of (3) are properly derived.

Some physical meaning can be given each of the terms on the right sides of the c.s.m. The first term of (16*a*) has the form of 'linear shoaling', that is, the result obtained from a W.K.B. treatment of the linear equations (5) on a mildly sloping bottom. It is present because of the

assumption that bottom slope is $O(\alpha)$. If bottom slope was deemed of higher order, the term would not appear in these equations, but would appear in a higher-order solution.

The first term of (16*b*) models the effect of $O(\alpha)$ dispersion. The term represents an increase in phase speed that is dependent weakly on depth and strongly on frequency, and is precisely the first correction to an expansion of the linear, finite-depth dispersion relation (2*c*) for small kh.

The remaining terms in the c.s.m. are due to nonlinear triad interactions. Since they are a sum over all possible interactions in which a given mode can participate, they represent the net rate of change of modal amplitude and phase. Viewed heuristically, a mode can be participating simultaneously in some triads in which it is gaining energy and in others in which it is losing energy. The ordering criterion of slow modal amplitude and phase changes must be satisfied for both the net changes and each individual triad interaction (Holloway 1980). Each of the interaction terms is composed of a quadratic product of amplitudes, a coupling coefficient, and a trigonometric term whose argument is a function of spatial phases only. For the evolution of phases (16*b*), the terms are further divided by the amplitude of the mode of interest. Phases thus have 'amplitude inertia' in that modes with small amplitude will tend to experience larger phase shifts, because of nonlinear interactions, than will larger amplitude modes (all else remaining equal). Note that if the dimensionless amplitude of any mode is initially $O(\alpha)$ and remains small for many interaction lengths, the formal ordering scheme is technically violated. Such a situation occurs for initial conditions described by very narrow-banded power spectra. In such cases, models similar to (16) predict only small, nonlinearly induced changes in the amplitudes and phases of modes whose frequencies are not near harmonics of the spectral peak. Although inclusion of small amplitude modes in $O(\alpha)$ rate equations such as the c.s.m. is not formally justified, comparisons between measured data and the formally inconsistent predictions of the c.s.m. are seen to be remarkably good (see §4(*b*)).

The coupling coefficients depend neither on the amplitudes nor on the phases of the interacting modes, but are functions of their frequencies, wavenumbers, and the local depth. For a given triad, the value of the coupling coefficient increases with decreasing depth.

The trigonometric term modulates the amplitude and phase changes according to the relative spatial phases of the three waves composing a given triad. At a position $x = D'$ the relative phase can be written

$$\Psi_j \pm \Psi_{\pm(n-j)} - \Psi_n = \int_0^{D'} \frac{\mathrm{d}}{\mathrm{d}x'} (\Psi_j \pm \Psi_{\pm(n-j)} - \Psi_n)\, \mathrm{d}x' + \Psi_j(0) \pm \Psi_{\pm(n-j)}(0) - \Psi_n(0).$$

Use of the definition (12*a*) and the dispersion relation results in

$$\Psi_j \pm \Psi_{\pm(n-j)} - \Psi_n = \int_0^{D'} \alpha(T_j \pm T_{\pm(n-j)} - T_n)\, \mathrm{d}x + \Psi_j(0) \pm \Psi_{\pm(n-j)}(0) - \Psi_n(0). \tag{18}$$

The importance of nonlinear phase changes over large distances is manifest in the integral on the right of (18). Although the integrand is formally $O(\alpha)$, if D' is $O(\alpha^{-1})$, the integral contributes an $O(1)$ amount to the relative phase. This affects both the magnitudes and signs of the amplitude and phase changes undergone by the interacting modes. Effects of the linear dispersion term in (16*b*) are also expressed through the trigonometric modulation term. Dispersion causes the phases of higher frequency modes to vary more rapidly with x than those of low frequency modes. The relative phase of a triad that contains high frequency modes will thus oscillate more rapidly than one that contains only relatively low frequency modes.

Consequently, the value and sign of the trigonometric term will change more quickly for the triad containing high frequencies, and net (over a scale $D' = O(\alpha^{-1})$) energy transfers and phase modulations will be smaller.

(*c*) *A dispersive shoaling model*

The dimensional equations (3) can alternatively be non-dimensionalized and scaled by

$$x' = h_0 x; \quad t' = (h_0/g)^{\frac{1}{2}} t; \quad \eta' = a_0 \eta; \quad \phi' = a_0 (gh)^{\frac{1}{2}} \phi; \quad h' = h_0 h, \tag{19}$$

which yields

$$\overline{\phi}_{xt} + \tfrac{1}{2}\epsilon(\overline{\phi}_x^2)_x + \eta_x - \epsilon h h_\xi \overline{\phi}_{xxt} - \tfrac{1}{3}h^2 \overline{\phi}_{xxxt} = 0, \tag{20a}$$

$$\eta_t + \epsilon h_\xi \overline{\phi}_x + h\overline{\phi}_{xx} + \epsilon(\eta \overline{\phi}_x)_x = 0, \tag{20b}$$

where $\epsilon = a_0/h_0 \ll 1$ and the bottom slope is $O(\epsilon)$. This set of equations, used by Mei & Unluata (1972) (the non-dimensionalization and scaling was apparently used implicitly by Peregrine (1972) in deriving his 'linearized Boussinesq equations') has only the nonlinear terms explicitly small; the dispersive term $\frac{1}{3}h^2\overline{\phi}_{xxxt}$ is formally of lowest order. The equations for $\epsilon = 0$ yield the counterpart of (7),

$$Q = a\sigma/hk^2, \quad k = (\sigma/h^{\frac{1}{2}})\,(1 - \tfrac{1}{3}h\sigma^2)^{-\frac{1}{2}}. \tag{21a, b}$$

The wavenumber k is no longer a linear function of σ. However, if $\frac{1}{3}h\sigma^2 \ll 1$, (21*b*) can be expanded and truncated to

$$k = (\sigma/h^{\frac{1}{2}})\,(1 + \tfrac{1}{6}h\sigma^2 + O(h^2\sigma^4)),$$

and the leading term is just shallow water dispersion. In terms of dimensional coordinates, the restriction $\frac{1}{3}h\sigma^2 \ll 1$ is not very severe for the physical shoaling problem: $\frac{1}{3}h\sigma^2 = 0.3$ corresponds to a wave period of about 6 s in 10 m depth, 4 s in 5 m depth, and a value of $(h/\lambda)^2$ (β of the previous discussion) of about 0.04. Thus although the system (20) formally has lowest order dispersion, the dispersion is mild for the wavelengths and frequencies encountered in the physical shoaling problem. In the following analysis we shall ignore the formal ordering problems associated with the fact that, with the present scaling, realistic values of σ and k will be small, and we will use the full dispersion relation (21*b*). Similar selective failure to neglect high order terms is not uncommon in the literature (see, for example, Grimshaw 1970; Bryant 1973), and occasionally has led to erroneous conclusions (cf. Johnson's (1973) comments regarding Grimshaw 1970). In §§4 and 5 we shall present experimental evidence suggesting that the major differences between a shoaling model derived from (20) and the c.s.m. derived from (4) are attributable to differences in linear dispersion relations. Linear, finite-depth theory will be seen to yield the best predictions of power and relative phase spectra in the regions of physical and frequency space where differences between the two nonlinear models are most apparent. As the linear dispersion relation (21*b*) is a better model of the finite-depth relation (2*c*) than is (7*b*), equations (21) will in fact be seen to provide a slightly better model for predictions of power spectra of sea–surface elevation than the more formally consistent equations (4).

Armstrong *et al.* (1962) and Bretherton (1964) showed that a system such as (21), with only mild lowest order dispersion, can be treated analytically by the methods described earlier for exactly resonant systems. Monotonic dispersion prohibits (in general) any triad from satisfying

both conditions (8) exactly. However, if the lowest order dispersion is mild, (8) can be satisfied with only small error by some triads. The conditions for this 'near resonance' are:

$$\pm\sigma_1 \pm \sigma_2 - \sigma_3 = \delta_\sigma, \quad \pm \boldsymbol{k}_1 \pm \boldsymbol{k}_2 - \boldsymbol{k}_3 = \boldsymbol{\delta}_k, \quad \delta_\sigma, \boldsymbol{\delta}_k \sim O(\epsilon). \tag{22a, b, c}$$

The formalism of (9)–(16) can easily be carried through (in the present case, $\delta_\sigma = 0$); the resulting evolution equations are:

$$\begin{aligned} Q_{n\xi} = &-\frac{Q_n k_n^2 h_\xi}{4\sigma_n^2} + \frac{1}{4\sigma_n^2}\sum_j Q_j Q_{(n-j)} \Gamma(k_j, k_{(n-j)}, j, n) \sin(\Psi_j + \Psi_{(n-j)} - \Psi_n) \\ &+ \frac{1}{4\sigma_n^2}\sum_j Q_j Q_{(j-n)} \Gamma(k_j, -k_{(j-n)}, j, n) \sin(\Psi_j - \Psi_{(j-n)} - \Psi_n) \\ &+ \frac{1}{4\sigma_n^2}\sum_j Q_j Q_{(j+n)} \Gamma(k_{(j+n)}, -k_j, j, n) \sin(\Psi_{(j+n)} - \Psi_j - \Psi_n); \end{aligned} \tag{23a}$$

$$\begin{aligned} T_n = &-\frac{1}{4Q_n\sigma_n^2}\sum_j Q_j Q_{(n-j)} \Gamma(k_j, k_{(n-j)}, j, n) \sin(\Psi_j + \Psi_{(n-j)} - \Psi_n) \\ &- \frac{1}{4Q_n\sigma_n^2}\sum_j Q_j Q_{(j-n)} \Gamma(k_j, -k_{(j-n)}, j, n) \sin(\Psi_j - \Psi_{(j-n)} - \Psi_n) \\ &- \frac{1}{4Q_n\sigma_n^2}\sum_j Q_j Q_{(j+n)} \Gamma(k_{(j+n)}, -k_j, j, n) \sin(\Psi_{(j+n)} - \Psi_j - \Psi_n); \end{aligned} \tag{23b}$$

where $\Gamma(k_1, k_2, j, n) = |k_1 k_2|(k_1 + k_2)\{h(k_j/\sigma_j)(k_1 + k_2) + \frac{1}{2}\sigma_n\}$. Equations (23) will be called the d.s.m. (dispersive shoaling model); they can be simplified and the coupling coefficients made symmetric by omitting terms of $O(\delta_k = \epsilon)$. The physical explanation of most terms is the same as for the c.s.m. However, (23*b*) lacks a second-order phase shift term (the first term on the right side of (16*b*)). The mild dispersiveness introduced by the term in (16*b*) is incorporated in the d.s.m. through the full dispersion relation (21*b*). The arguments of the trigonometric modulation terms are now given by

$$\begin{aligned} \Psi_j \pm \Psi_{\pm(n-j)} - \Psi_n = &\int_0^{D'} (k_j \pm k_{\pm(n-j)} - k_n)\,\mathrm{d}x \\ &+ \int_0^{D'} \epsilon(T_j \pm T_{\pm(n-j)} - T_n)\,\mathrm{d}x + \Psi_j(0) \pm \Psi_{\pm(n-j)}(0) - \Psi_n(0). \end{aligned} \tag{24}$$

From (22*b*), $(k_j \pm k_{\pm(n-j)} - k_n) = O(\epsilon)$; on a flat or mildly sloping bottom where the wavenumbers are only slowly varying functions of x, the effect of the mismatch in the resonance condition is to introduce slow changes in the relative phase of the triad similar to the linear phase shift term in the c.s.m. The larger the mismatch, the more rapid are the relative phase oscillations. Since the deviation from linearity of the dispersion relation (and hence the mismatch) is more pronounced at high frequencies, net energy transfers and phase changes are expected to be small for triads containing high frequency modes. It is thus reasonable to suppose that a high frequency cutoff in the sums (11) is possible; as long as it is sufficiently high, the exact cutoff frequency is not critical (Bretherton 1964). Of course, as depth decreases, the linear modes become more non-dispersive in character. In the limit of extremely small depth, all modes have vanishing mismatch, and the cutoff frequency must be extremely high (cf. Nayfeh 1981). In this limit, however, both the governing equations (3) and the perturbation-solution techniques are inappropriate and should be replaced by the nonlinear shallow water equations and one of the many techniques for obtaining approximate solutions of hyperbolic equations (Whitham 1974; Nayfeh 1981).

PHILOSOPHICAL TRANSACTIONS OF THE ROYAL SOCIETY A MATHEMATICAL, PHYSICAL & ENGINEERING SCIENCES

Neither the c.s.m. nor the d.s.m. have known analytic solutions. If the depth is constant and only a single resonant triad is considered, Armstrong *et al.* (1962) and Bretherton (1964) show that solutions exist in which modal amplitude and phase variations are described by Jacobi elliptic functions. These solutions are applicable to a system composed of many discrete modes only when ϵ (and hence $\delta_k = O(\epsilon)$) is so small that any given mode participates in at most a single near resonant triad (Bretherton 1964). This is clearly not the case for shoaling surface gravity waves. The evolution equations must thus be integrated numerically.

In the present study we have implemented a numerical scheme known as 'repeated extrapolation to the limit' due to Gragg (1963) and Bulirsch & Stoer (1966) (see Stoer (1972) for a review of extrapolation methods and improvements on the original algorithms). The algorithm is both efficient and highly accurate and is easily modified to accommodate large numbers of coupled equations. We have performed extensive testing and have verified the accuracy and consistency of the numerical scheme for the evolution equations given above. In addition, we have monitored the conservation of lowest-order energy flux for all integrations; in no case did total (spectrally integrated) lowest order energy flux vary by more than 0.01 % in the course of any integration through the entire shoaling region.

3. Experiment

A field experiment to measure the wave parameters of sea–surface elevation, pressure, and horizontal velocity was undertaken at Torrey Pines Beach, California, during the summer and autumn of 1980. The primary goal of the field work was to determine the operational validity of the one-dimensional shoaling models developed in the previous section. However, the dearth of existing quantitative wave measurements in the shoaling region motivated an extension of purpose. The experiment was also designed to provide a comprehensive, quantitative description of wave-induced fluid motions throughout the shoaling region, with the hope that the data would be useful for testing future shoaling theories. To this end, the on–offshore measurements were extended beyond the defined shoaling region (10 m–3 m depth), and two, two-dimensional arrays of instruments were established at different depths to allow measurements of wave frequency–directional spectra.

This section describes the experimental site and instrumentation, experiment design and sensor placement, and data acquisition and reduction.

(*a*) *Site and instrumentation*

Torrey Pines Beach, California, has been the site of numerous nearshore field experiments (Pawka *et al.* 1976; Aubrey 1978; Gable 1979; Inman *et al.* 1980). Located approximately 3 km north of Scripps Pier, it is readily accessible both by small boat and four-wheel-drive vehicle. The bathymetry is relatively homogeneous in the longshore direction, with contours aligned on a heading of approximately 353.5° true. The beach is composed of fine, quartz sand (mean diameter 0.17 mm) and has a nearly constant slope of 2.2 % through the shoaling region. Extensive studies of the wave climate at the site were reported by Pawka *et al.* (1976) and Pawka (1982).

Twenty-eight channels of wave data were obtained from three types of instruments: 10 pressure sensors, 5 dual-axis electromagnetic current meters, and 8 surface-piercing resistance wavestaffs. The pressure sensors used were of the strain gauge type, predominately Statham

model PA 506-33 (a limited number of Transducer, Inc. no. 5AP-69F-50 were also used). The pressure sensors were extremely durable and easy to install and maintain when mounted in the standard configuration, approximately 25 cm above the bottom. Previous experience had shown them to be highly linear and virtually drift-free over long periods of time and under varying ocean conditions.

The linearized form of Bernoulli's equation can be used to relate pressure signals directly to sea–surface elevation or horizontal current speed when finite-amplitude effects are locally small. Pawka *et al.* (1976) and Guza & Thornton (1980) present comparisons between estimates of wave parameters derived from co-located pressure sensors, wavestaffs, and current meters throughout the shoaling region and surf zone. In most cases reported, agreement between pressure-derived estimates of sea–surface elevation and direct measurements was well within 10% in amplitude across the entire wind wave frequency band. The agreement was virtually independent of spectral shape, total variance, and on offshore–position, with the exception of the region close to the onset of breaking. In place of the linearized Bernoulli equation, the relations obtained from the linearized Boussinesq equations can be used with comparable results everywhere except at frequencies greater than 0.17 Hz in water deeper than 9 m. (The discrepancy in these regions arises from the breakdown of the long wave assumptions inherent in the derivation of the Boussinesq equations.) The linear, finite-depth theory (Bernoulli's equation) was used in the present study to provide sea–surface elevation estimates from bottom pressure measurements.

The current meters used were Marsh–McBirney no. 512 dual axis, electromagnetic current meters. The instruments measure two orthogonal components of velocity. In this experiment, the sensing elements were placed approximately 1 m above the bottom, and the longshore and on–offshore components of horizontal velocity were measured. Although they are rugged and durable, there is considerable uncertainty about the response of the instruments to a broad-banded wave field (Lavelle *et al.* 1978; Cunningham *et al.* 1979). Uncertainty in orientation (about 5° in all directions) further degraded the current meter data. The performance of the meters was a disappointment throughout the course of the experiment. Apparent gain reductions of up to 30% were observed to occur over immersion periods of about one month. The changes became apparent only when new, dry meters were substituted for ones that had been under water for some time. Because of the questionable gains, it was decided to ignore all current meter data for the comparisons with the shoaling models presented here. Since various types of instruments were intermingled on the on–offshore line, the loss of all current meter data was not catastrophic. It did, however, seriously affect the high frequency aliasing characteristics of the directional arrays discussed below.

The wavestaffs used were similar to those described in Flick *et al.* (1979) and consisted of twin nichrome resistance wires supported vertically by a fiberglass pole 5 m long. The staffs are useful for direct measurements of sea–surface elevations in mean depths shallower than about 6 m. As with the pressure sensors, considerable field testing has shown these instruments to be linear and stable, with excellent high frequency response to 10 Hz.

(*b*) *Experiment design and sensor placement*

Quantitative comparison of the one-dimensional shoaling models' predictions with data required instrumentation of an on–offshore transect through the shoaling region, approximately 300 m in horizontal extent. Based on the results of Guza & Thornton (1980), spatial coverage

was maximized by placing only a single instrument at each on–offshore location; the linear, finite-depth relations were used to transform locally from the measured variable to the wave variable of interest on a frequency band-by-band basis.

Previous data obtained on the same beach in November, 1978 (Gable 1979; Guza & Thornton 1980), as well as casual observation, indicated that the evolution of the wave field became pronounced in shallow water, as opposed to rather mild evolution observed near the deeper, seaward edge of the shoaling region. This is entirely consistent with the forms of the c.s.m. and d.s.m., in which modal amplitudes, coupling coefficients, and closeness to resonance all increase with decreasing depth. Thus, rather than sampling evenly along the on–offshore transect, the density of instruments was greater in shallow water, primarily at the expense of

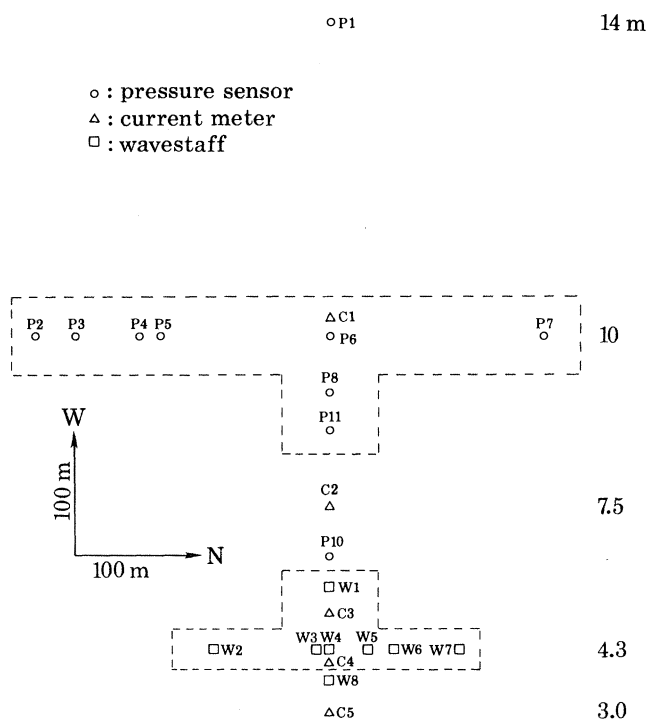

FIGURE 2. Plan view of the instrument locations in the 1980 shoaling waves field experiment. Approximate depths are given near the right side of the figure.

the mid-depth (8–6 m regions). As seen in the plan view figure 2, a mix of 4 pressure sensors, 5 current meters, and 3 wavestaffs constituted the main on–offshore instrumentation. Wavestaffs were used in shallow water in place of pressure sensors, in part to avoid complications arising from previously observed discrepancies (near the break zone) between direct measurements of sea–surface elevation and estimates inferred from pressure data; however, under most wave conditions, the instrumentation did not extend to the break zone.

A pressure sensor (P1) was placed some 240 m seaward of P6 in a depth of 14.5 m. P1 was mounted 4.3 m above the bottom, considerably higher in the water column than other sensors, in order to minimize depth attenuation of signals from high-frequency wind waves. If the evolution of the wave field was truly dominated by nonlinear triad interactions as hypothesized, the interactions were expected to be very weak over large portions of the wind wave frequency

band in water deeper than 10 m. At these relatively large depths, quantitative predictions of the Boussinesq models were expected to diverge from the actual data, in consequence of the breakdown of the long wave assumptions. However, the inability of the wave field to approximately satisfy the conditions (8) in deep water was expected to hinder net nonlinear transfers via the triad mechanism. As discussed in §1, nonlinear energy exchanges should then occur on the much larger length scales appropriate to the quartet mechanism of Phillips (1960). The primary function of the deep sensor P1 was to verify this qualitative reasoning.

The field experiment was designed to measure wave directional spectra at two depths in the shoaling region. A well-surveyed, five sensor, linear array of pressure sensors (instruments

TABLE 1. POSITIONS AND APPROXIMATE UNCERTAINTIES FOR SENSORS IN THE SHOALING WAVES FIELD EXPERIMENT

(Positions are given in metres relative to a left-handed coordinate system centred on an arbitrary benchmark on the beach, with the positive Y-axis aligned with true North (thus approximately longshore). Uncertainties are given in metres, and apply to both the X- and Y-coordinates.)

name	X/m	Y/m	uncertainty/m
P1	794.6	475.6	4.0
P2	527.5	270.0	0.5
P3	531.6	300.9	0.5
P4	536.4	351.5	0.5
P5	538.1	369.2	0.5
P6	553.4	501.5	0.5
P7	573.4	665.2	0.5
P8	507.0	506.2	1.5
P10	389.0	518.3	2.0
P11	478.9	509.0	1.5
C1	567.4	500.1	1.0
C2	425.0	514.1	2.0
C3	337.6	523.9	1.0
C4	301.8	529.8	0.5
C5	227.7	516.0	2.0
W1	359.9	520.9	0.3
W2	296.9	439.0	0.3
W3	307.7	516.5	0.3
W4	308.5	527.7	0.3
W5	310.3	557.3	0.3
W6	313.8	575.3	0.3
W7	320.8	629.2	0.3
W8	287.3	528.2	0.3

P2, P3, P5, P6, and P7, see figure 2) had been established at the Torrey Pines site in March 1977. Design criteria and analysis techniques for this array are discussed in detail by Pawka (1982). The array had a total longshore extent of 396 m. The original five sensor array had minimum lag spacing of 33 m, corresponding to an aliasing frequency of 0.16 Hz in 10 m depth (Pawka 1982). Addition of another sensor (P4) reduced the minimum lag to 17.8 m and the aliasing frequency to 0.20 Hz. This is approximately the operational high frequency limit imposed by depth attenuation of the pressure signal itself. Addition of P4 also allowed use of the four sensor subarray P2–P3–P4–P5 with optimal lag spacing 1–3–2 (Barber 1961) in the event that sensor locations P6 and P7 could not be supported: however, the anticipated problems fortunately did not materialize, and use of the shortened array was not necessary.

A second directional array was designed to operate in a mean depth of approximately 4 m.

The heart of this instrument group was a 1–3–2 longshore array of wavestaffs, with basic lag 10 m. The array thus had aliasing characteristics similar to those of the deep array. Provision was made for two additional sensors in the longshore, and model testing with realistic spectra led to the final longshore array design 8–1–3–2–5, with a total length of 190 m.

All linear wave gauge arrays suffer from 180° directional ambiguity with respect to the line connecting the sensors. The historical justification for the use of linear longshore arrays in coastal regions has been the assumption, which was avoided here, of no seaward–propagating energy in the wind wave frequency band. In the plan view figure 2, all sensors enclosed within a set of dashed lines could be analysed as a single, two-dimensional directional array. Such an array theoretically allows unambiguous resolution between seaward- and shoreward-propagating energy in a given frequency band. Some results from a directional analysis will be discussed in §5; model testing with realistic synthetic spectra and the maximum likelihood estimator was used as an aid in array design.

With the exception of a few previously established sensor sites, all sensor locations were initially determined with a mini-ranger locating system operated from a small boat. Positions were later verified by numerous mini-ranger surveys and direct, underwater measurements between instruments. All wavestaff locations were further refined by standard surveying from known benchmarks on the beach. The position and approximate uncertainty for each sensor is given in table 1.

(*c*) *Data acquisition and reduction*

The sensors were divided into two groups for data acquisition purposes. All sensors seaward of P11 (inclusive) received their power from, and returned signals to, a tethered spar as described by Lowe *et al.* (1972). An electronics package inside the spar scanned each data channel at 64 Hz. On each scan, all analogue data were digitized, encoded (with a pulse code modulation scheme), multiplexed, and transmitted over a v.h.f. radio link to the Shore Processes Laboratory, where the telemetered data stream was recorded directly on magnetic tape.

A similar scheme was used for data from all sensors shoreward of P11. An underwater electronics package located near site W4 distributed power and performed signal conditioning as described above. Digitized, encoded data were returned to a beach installation via a single cable. The data stream was then transmitted over a separate v.h.f. link to the laboratory, where it was recorded on magnetic tape simultaneously with the deep station's data and additional timing information. In a separate, non-real-time operation, data from the raw telemetry tape were decoded, demultiplexed, block-averaged to a sampling rate of 2 Hz, and placed on to computer-compatible magnetic tape. Further preliminary processing removed rare 'glitches' (caused, for example, by brief telemetry signal losses) and applied a low-pass digital filter with cutoff frequency 0.9 Hz.

The data presented and analysed in the following sections were obtained over a two week period in early September 1980. During this time all pressure sensors and wavestaffs were operational. Continuous data was obtained for between 10000 and 26000 s on 11 separate occasions. Tidal variations during data runs ranged between 20 and 100 cm (runs were taken across all stages of the tidal cycle). The average variance of sea–surface elevation in the wind wave band (as measured in 10 m depth) was approximately 90 cm² in early September, grew to 510 cm² as wave energy from a storm in the southern hemisphere arrived, and then decreased to 175 cm² by 16 September. Spectral shape varied considerably over the two weeks

PHILOSOPHICAL TRANSACTIONS OF THE ROYAL SOCIETY A MATHEMATICAL, PHYSICAL & ENGINEERING SCIENCES

of interest. An intensive bathymetric survey was conducted on 9 September, and measurements of instrument heights off the bottom indicated that the bathymetry of the shoaling region remained relatively constant throughout the period of interest.

4. Data comparison

In this section we present comparisons between data obtained in the field experiment, predictions of the nonlinear c.s.m. and d.s.m., and predictions of slowly varying, linear finite-depth theory (l.f.d.t.) as described in Chu & Mei (1970). Before making such comparisons, however, fundamental assumptions regarding the statistical nature of the wave field must be made. Specifically, the c.s.m. and d.s.m. derived in §2 are deterministic: they assume that the wave field is composed of a finite number of discrete modes, each having a fixed frequency and definite amplitude and phase. Nonzero frequency spacing between discrete modes is crucial for simultaneously preserving the asymptotic validity of the expansions (9) and the two-scale assumptions (11) and (12).

Uniformly valid solutions of the fully statistical problem posed by a weakly nonlinear system with a continuous spectrum are achieved only at the expense of considerable added complexity (cf. Newell 1968). (Even with such treatments, it is not clear that precise comparisons between theory and data can be obtained, owing to the necessarily finite duration and extent of any data.) In the following analysis, the deterministic c.s.m. and d.s.m. are used to predict various statistics of the surface gravity wave field in the shoaling region. Inputs to the models, such as the number of modes, their frequencies, initial amplitudes, and initial phases, were obtained from the data in arbitrary ways discussed below. Power, coherence, and phase spectral estimates have been stabilized by averaging over both frequency bands and data records ('ensemble averaging'). These techniques are strictly applicable only when applied to time series that are realizations of ergodic random processes. Considerable care has been taken to insure that differences between the outputs of the various models, and between the models and the data, can be ascribed to the deterministic 'physics' contained (or lacking) in the models, rather than to either the time series analysis techniques used or the choice of deterministic initial conditions. An extensive series of numerical simulations with realistic but synthetic 'data' indicated that the c.s.m. and d.s.m. predictions of smoothed power spectra, as well as smoothed coherence and relative phase between the models and the 'data', were insensitive to the number of modes used to represent the wave field. (In all simulations, the number of modes chosen was sufficient to define significant spectral features; in this sense, although all spectra were necessarily discrete, they were smooth.) These simulations also showed an insensitivity to the details of how smoothed spectra were obtained; frequency merging and ensemble averaging yielded very similar results.

Three selected field data sets have been compared with predictions of the models. The three sets encompass a wide range of wave energies and spectral shapes. For each data set, time series from the on–offshore sensors P1, P6, P8, P11, P10, W1, W4, and W8 were broken into consecutive records of 1024 s duration. These records were then fast Fourier transformed and, where appropriate, Fourier coefficients of near bottom pressure were converted to coefficients of sea–surface elevation (s.s.e.) by using the linear, finite-depth transformation; 240 modes evenly spaced in the frequency band 0.001–0.234 Hz were used to represent the wave field through the shoaling region. The Fourier coefficients of s.s.e. obtained from sensor P6 in

approximately 10 m depth provided initial modal amplitudes and phases of depth averaged velocity potential by using the appropriate linear transformation (7*a*) or (21*a*). Although this procedure introduces small errors to the initial conditions, it can be shown that these errors cannot significantly affect the evolution of the wave field over distances comparable with the extent of the shoaling region. By using the initial conditions, the model equations were integrated numerically to produce predictions of Fourier coefficients at the six onshore sensor

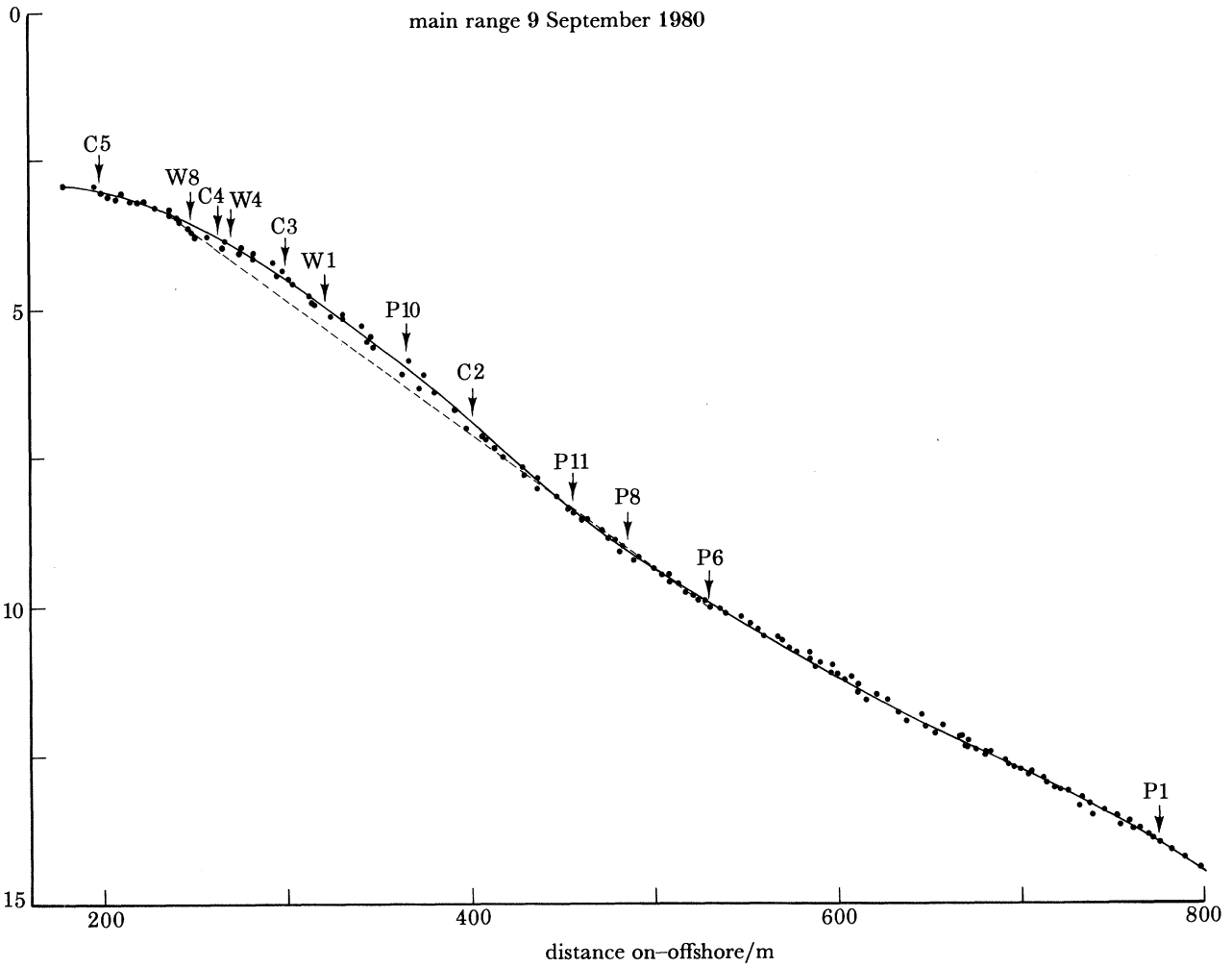

FIGURE 3. On–offshore bathymetry and sensor locations along the main instrument transect. The dashed line represents the plane beach with slope 0.022 used in the model integrations. On–offshore distance (in metres) is relative to an arbitrary benchmark.

locations. Although detailed measurements of bottom topography were available, the numerical integrations were carried out with constant bottom slope of 0.022. This assumed linear dependence of depth on on–offshore position allowed calculation of the spatial phase $\Psi_n(x)$ in closed form for both the c.s.m. and d.s.m., thus greatly simplifying the numerical integrations. As the coupling coefficients and dispersion relations appropriate for the nonlinear models contain only weak depth dependence, and as the beach of interest is in reality nearly plane, it was not expected that the results would differ significantly from those obtained by using real topography

in the integrations. Figure 3 shows the measured on–offshore topography along the main range of instruments, the plane topography used in the integrations, and the sensor positions. The initial depth was obtained directly from the mean pressure measured at P6, and thus varies in accordance with the tides.

Since the integrations yield predictions of Fourier coefficients, not simply spectral quantities, it is reasonable to examine the correlations between time series predicted by the models and those obtained from the data. In the frequency domain, such information is contained in the coherence and relative phase spectra (Jenkins & Watts 1968). If the smoothed cross spectrum between two time series p and q is $C_{pq}(f)$, then the coherence $\gamma_{pq}(f)$ is

$$\gamma_{pq}(f) = [C_{pq}(f)\, C^*_{pq}(f)/C_{pp}\, C_{qq}]^{\frac{1}{2}}, \tag{25}$$

$0 < \gamma < 1$ is a measure of the correlation between the bandpassed time series p and q. The smoothed phase $\theta(f)$ between the time series is defined by

$$\theta_{pq}(f) = \arctan\,[\mathrm{Im}\,(C_{pq})/\mathrm{Re}\,(C_{pq})]. \tag{26}$$

If phases are positive, then the series p leads q.

Smoothed power spectra of s.s.e. were constructed for each data set and the resulting model integrations. Coherence and relative phase spectra between model predictions and the data were also analysed. Smoothing in the frequency domain was accomplished both by ensemble and frequency averaging. Chi-squared testing of unsmoothed spectral estimates (Haubrich 1965) indicated that the statistics of all data sets analysed below were stationary over the time scale of the data.

(*a*) 5 *September*

The 5 September data set consists of 11 records (11 264 s) obtained on a mildly rising tide. It is typical of the low energy (93 cm^2 variance measured in 10 m depth), broad-banded (in frequency) wave conditions common at the site throughout the summer. Figure 4 presents averaged spectra of s.s.e. observed at the four locations P1, P6, W1, and W8. The spectrum is basically flat from 0.125–0.25 Hz, with two narrow, but not very energetic peaks centered at 0.053 and 0.077 Hz.

The spectra measured at locations P1 (14 m depth) and P6 (10 m depth) are virtually identical. This is expected since linear shoaling effects are negligible and near resonant triad interactions are small due to large mismatch terms in this rather deep water. From approximately 0.15–0.25 Hz, the spectra exhibit no systematic differences through the shoaling region. From 0.05–0.15 Hz, spectral shape does not change appreciably through the shoaling region. However, there is a smooth, mild increase in spectral density with decreasing depth.

Figure 5 presents comparisons between data and model predictions of averaged spectra of s.s.e. at the six on–offshore locations. At each location, spectra obtained from the data, the c.s.m., the d.s.m., and linear, finite-depth theory have been plotted. Each spectrum has 160 degrees of freedom, and the 90% confidence limits (Jenkins & Watts 1968) are shown. At all locations through the shoaling region, linear finite-depth theory (l.f.d.t.) accurately models the observed spectrum of s.s.e. The d.s.m. is slightly worse only at frequencies greater than 0.18 Hz, where the model consistently underpredicts spectral density. These results are in contrast with the c.s.m., which overpredicts spectral density in a wide frequency band from 0.12–0.24 Hz.

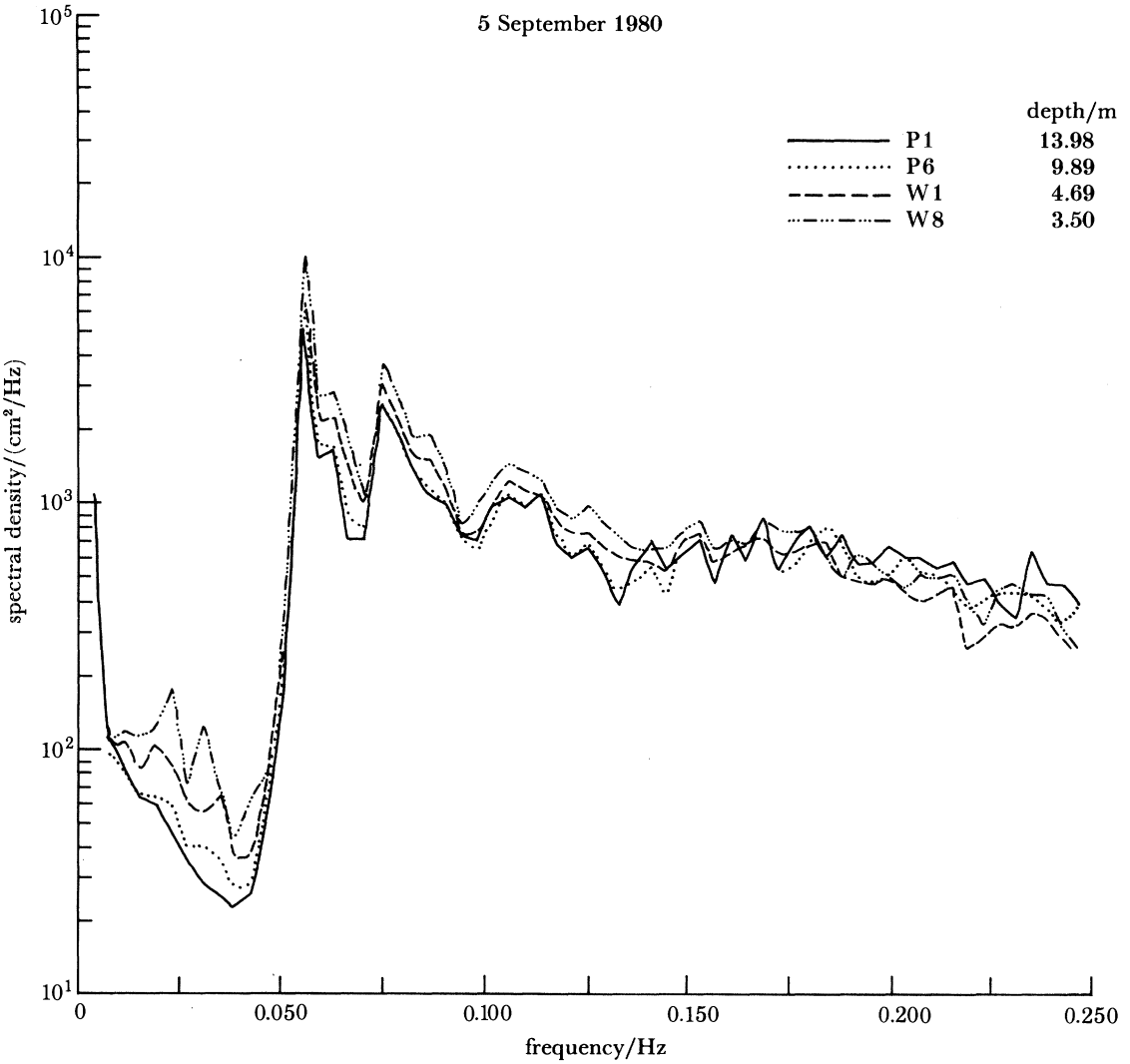

FIGURE 4. Averaged power spectra of sea-surface elevation measured at 4 on–offshore locations. Averaged bandwidth is 0.0039 Hz. Location names and mean depths (metres) are shown.

Additional information can be obtained by comparing coherence and phase spectra between the nonlinear models and l.f.d.t., and the data. Figure 6 presents smoothed coherence spectra through the shoaling region. For both l.f.d.t. and the nonlinear models, coherence with the data is greater than 0.9 throughout the low frequency region of the wind spectrum (0.05–0.1 Hz). At higher frequencies, the dominant feature of the coherency spectrum is a pronounced decrease in coherence with increasing frequency. Such a feature is present to some extent in all of the data analysed to date, and is consistent with the observed finite directional spread of the wave field. Model testing was carried out with a constant depth shoaling region and a wave field obeying l.f.d.t. Directional spectra $E(f, \theta)$ were obtained from a maximum likelihood estimator analysis of data from the shallow longshore array of wavestaffs W2–W7. Briefly, the cross spectrum at lag r in the on–offshore can be determined if the wave field is homogeneous and the directional spectrum $E(f, \theta)$ is known:

$$C(f, r) = \int E(f, \theta)\, \mathrm{e}^{\mathrm{i}k(f)\, r \cos(\theta)}\, \mathrm{d}\theta \qquad (27)$$

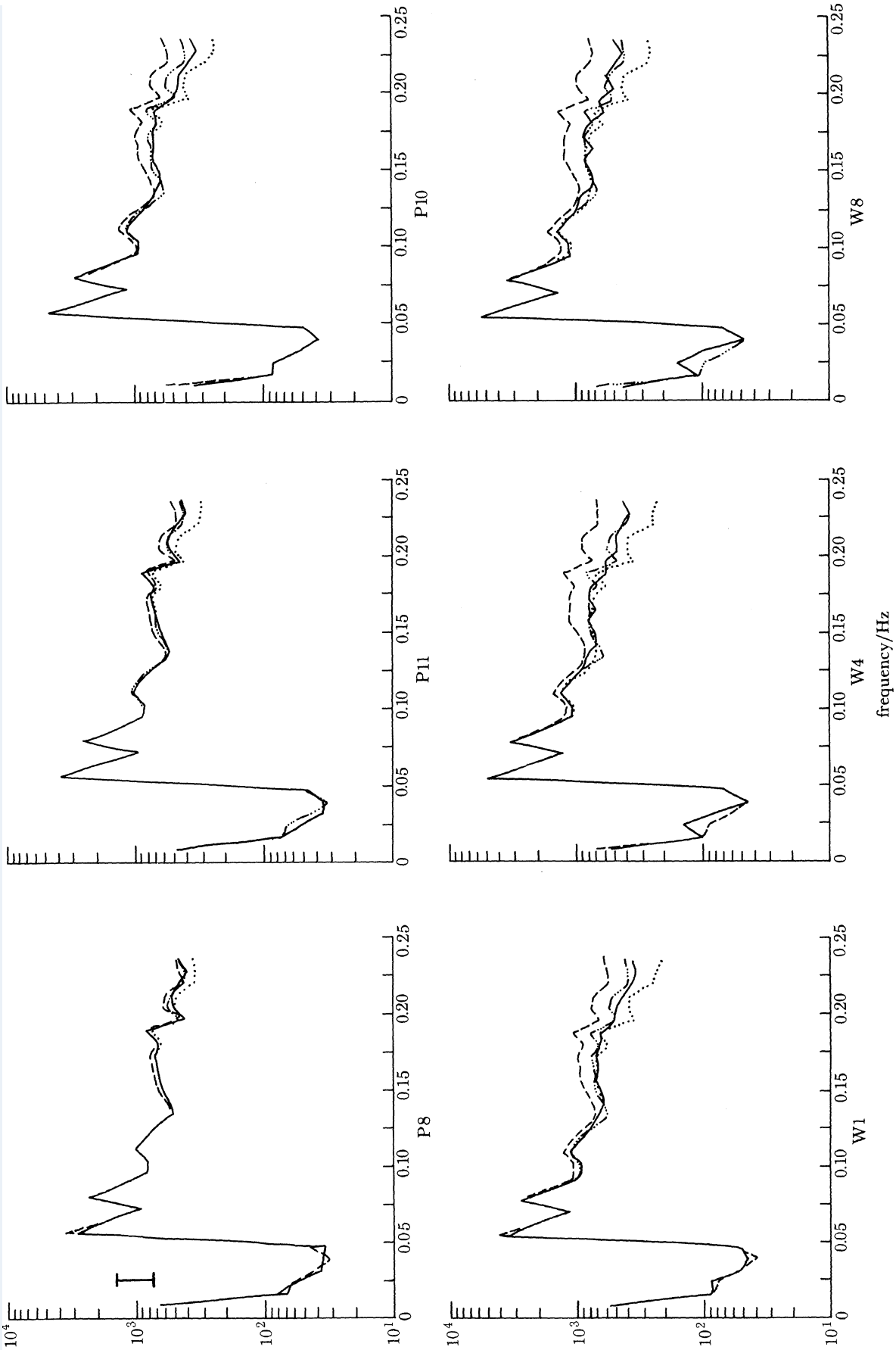

FIGURE 5. Comparison of averaged power spectra of sea-surface elevations between measured data (——), the d.s.m. (· · ·), the c.s.m. (– – –) and linear, finite-depth theory (l.f.d.t.) (—·—·—). Averaged bandwidth is 0.0078 Hz. All model input conditions were derived from data measured at P6. Shown under each plot are the location name and its on–offshore distance from the initial conditions. The abscissa is frequency (Hz) and the ordinate is spectral density (cm²/Hz). Spectra have the equivalent of 160 degrees of freedom and the 90 % confidence limits are shown on the plot for P8.

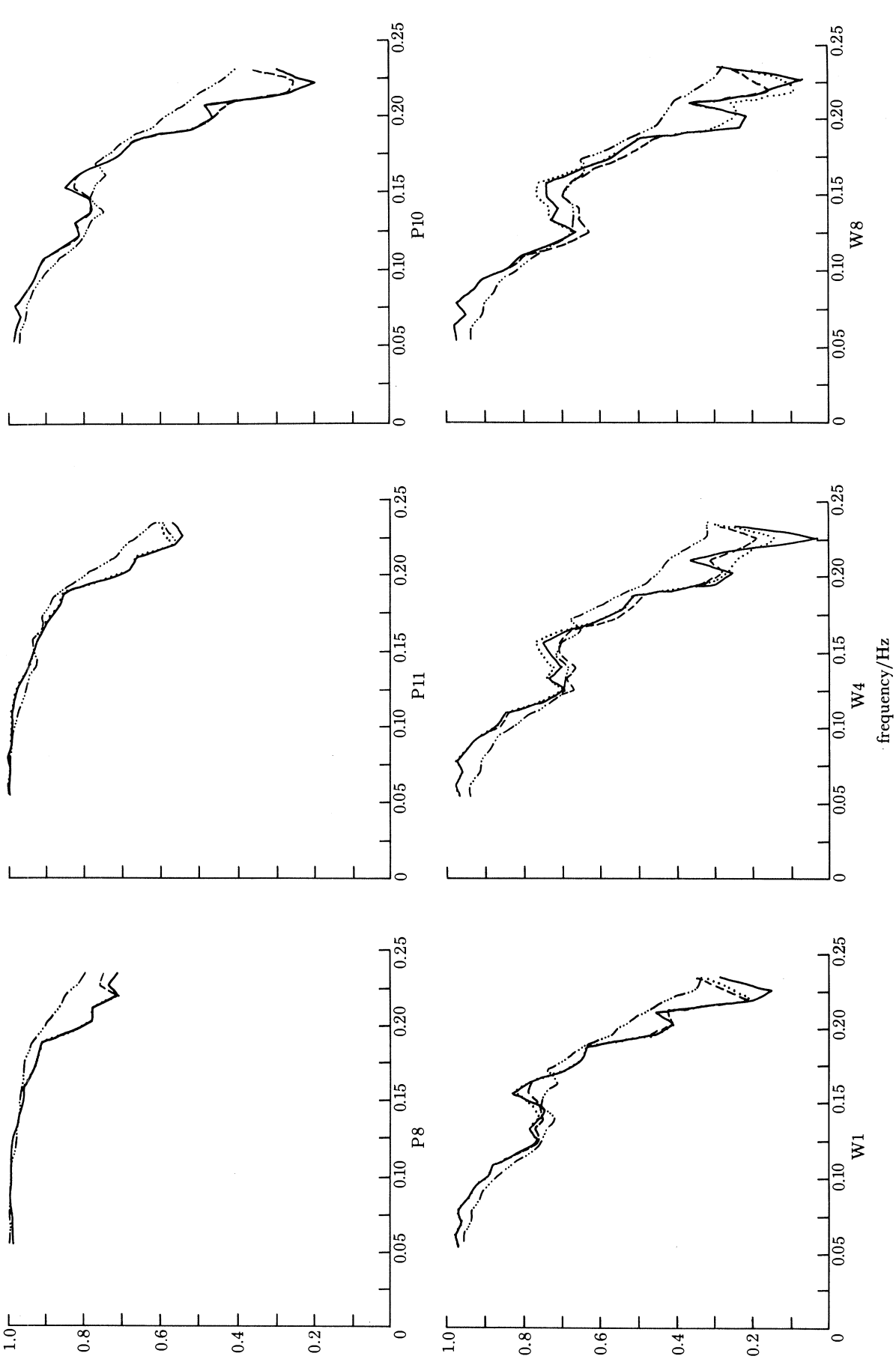

FIGURE 6. Comparison of smoothed coherence between predictions of the d.s.m. (——), the c.s.m. (···), linear, finite-depth theory (l.f.d.t.) (– – –) and the data at the 6 on–ofishore locations of figure 5. Also shown (TEST, –·–·–) is the coherence predicted by assuming a uniform, 5 m depth shoaling region and linear waves with the measured directional spectrum obtained from the array W2–W3–W4–W5–W6–W7. Note that the ordinate is coherence (*not* coherence squared).

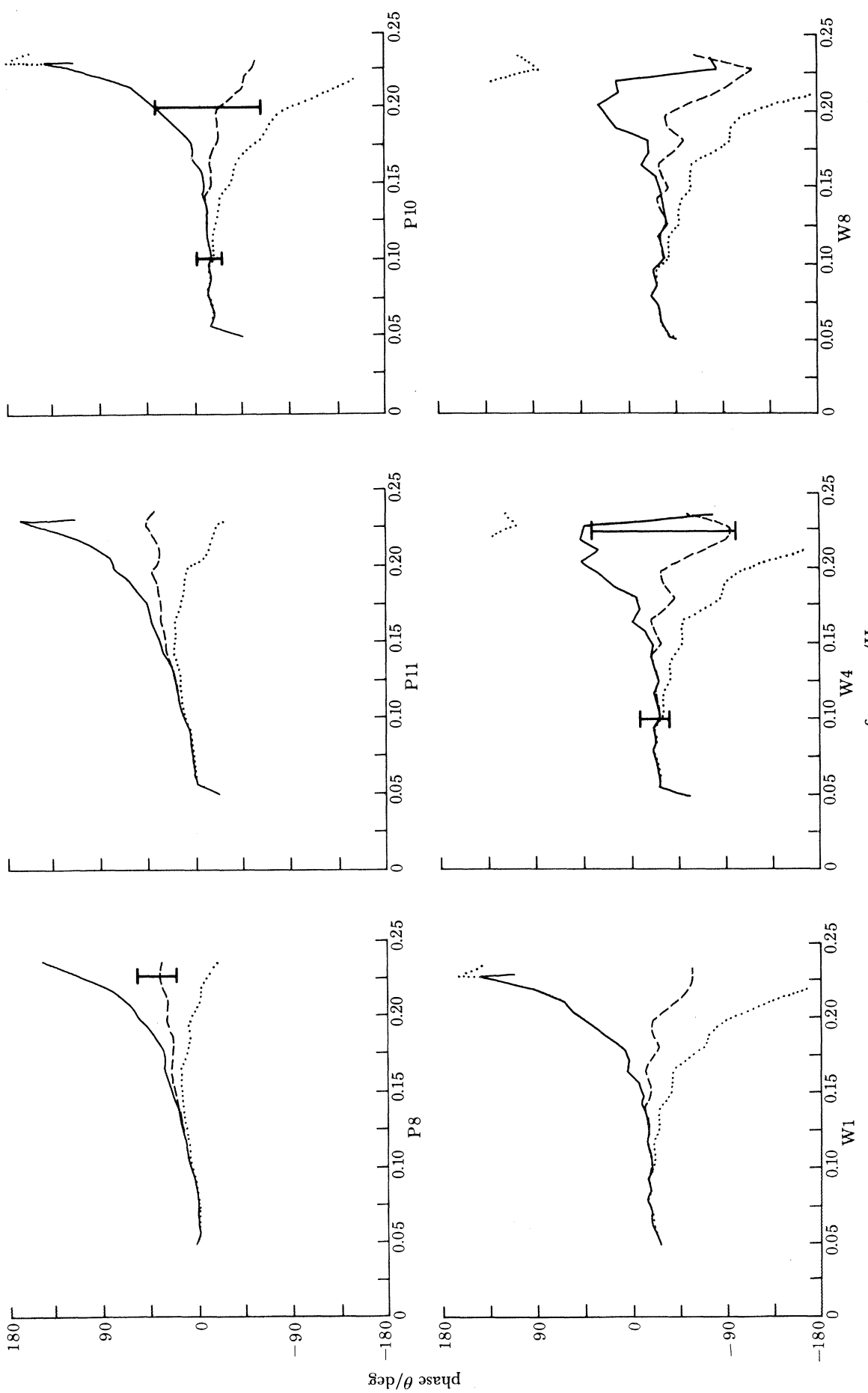

FIGURE 7. Comparison of relative phase spectra between predictions of the shoaling models and the data. Relative phase is shown in degrees; 90% confidence limits in phase (nearly the same for all three models (d.s.m., —; c.s.m., ···; l.f.d.t., – – –)) are shown for various frequencies at different on–offshore locations.

(Cartwright 1962). By using the definition (25) and calculating the integral in (27) numerically, test coherence spectra (labelled TEST in figure 6) can be generated. The general shape of the test spectra was found to be neither a strong function of the assumed depth nor of the detailed fine structure of the directional spectrum estimates.

The test coherence spectrum is quite similar to the model-data coherences, even including the slight plateau observed at 0.15 Hz. The dramatic fall-off of the coherence spectra with increasing frequency and onshore distance can thus be attributed to the effects of increased

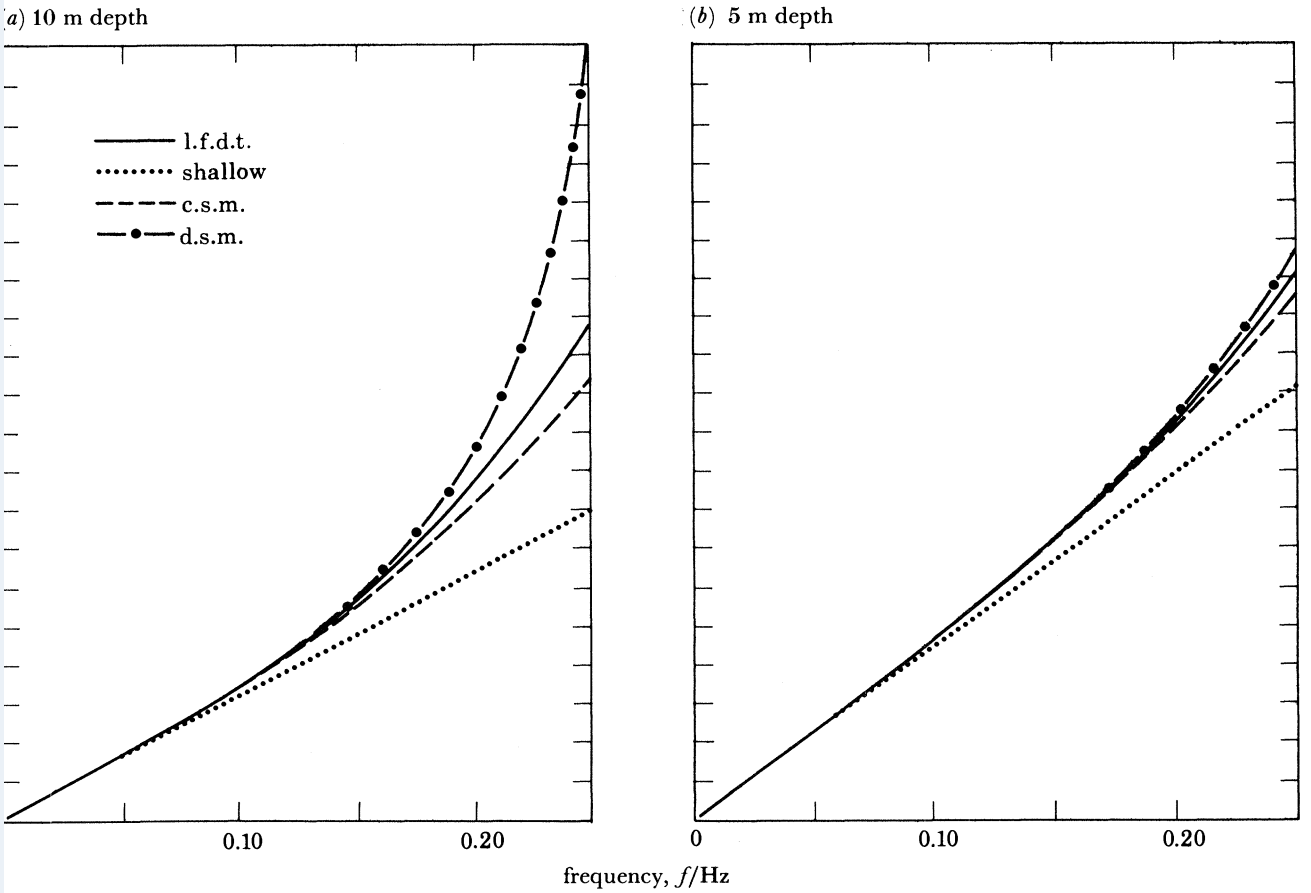

FIGURE 8. Wavenumber against frequency for four linear dispersion relations at two depths. (*a*) 10 m; (*b*) 5 m. The d.s.m. is equation (21*b*), c.s.m., is effective total linear wavenumber for the c.s.m., l.f.d.t. is equation (2*c*), and shallow is non-dispersive shallow-water theory (equation (7*b*)).

directional spread in the higher frequencies and the fact that a given spatial lag represents a larger normalized (by wavelength) lag for higher frequency waves than for lower frequency ones. Additional model testing, in which the shape of the directional spectrum was not assumed to be a function of frequency, indicated that the second effect was dominant.

There are no significant deviations in coherence between any of the shoaling models tested. The good agreement for spectral and coherence predictions between linear and nonlinear models and the data strongly indicates that net nonlinear effects are small through the shoaling region for this particular data set. The phase spectra, presented in figure 7, can thus be interpreted for this data set in terms of the linear dispersion relations appropriate for the c.s.m.,

the d.s.m. and l.f.d.t. It should be borne in mind throughout the phase discussion that confidence limits on the phase estimates are dependent on the coherence, and thus phase estimates at the higher frequencies in shallower reaches of the shoaling region are extremely uncertain. As the coherences for all models are virtually identical everywhere, confidence limits on the phase estimates have been included on figure 7.

L.f.d.t. phases at locations P8 and P11 are nearly consistent with zero phase shift at all frequencies. (The very slight trend of increasing phase with increasing frequency is possibly due to a small uncertainty in sensor positions.) Both of the nonlinear models show large deviations from the data, especially at high frequencies. The d.s.m. shows a strong tendency to lead the data while the c.s.m. has a lesser tendency to lag, although both models agree well with the data at lower frequencies. The deviations are consistent both in sign and magnitude with differences between the linear dispersion relations (2*c*), (7*b*), and (21*b*). The relation (21*b*) grossly overpredicts wavenumber for high frequency waves in relatively deep water, as shown in figure 8. Thus, the linear contribution to total phase $\Psi_n(x)$ will be larger than that predicted by l.f.d.t., and the d.s.m. will lead the l.f.d.t. prediction. The second-order linear phase change term, as well as the linear dispersion relation, must be taken into account when considering the c.s.m. However, the magnitude of the linear phase change term is insufficient to offset the dispersion relation's underprediction of wavenumber at high frequencies in deep water (figure 8), which leads to the observed lag of the model in relation to l.f.d.t. (and hence, in this case, the data).

(*b*) 11 *September*

The second data set consists of 20480 s of data obtained on 11 Sptember over a tidal maximum. With total variance in 10 m depth of over 500 cm², this data set is the most energetic analysed for this work. As seen in figure 9, the vast majority of the energy in the wave field at depths greater than 10 m is concentrated in a narrow band centered about 0.065 Hz, representative of long period, well directed swell. In §5 we discuss the frequency-directional characteristics of this data set. Significant spectral evolution occurs as the waves propagate shoreward, as is evident in figure 9. In shallow water, a secondary (but significant) peak is observed centred at 0.127 Hz, nearly the exact second harmonic of the primary peak in the power spectrum. As in the 5 September data set (figure 4), no significant spectral evolution is observed between locations P1 in 14.5 m depth and P6 in 10 m depth.

Figure 10, similar to figure 5, compares averaged spectral predictions of the nonlinear models and l.f.d.t. with the data. The smooth, steady growth of the secondary peak at 0.127 Hz is modelled almost precisely by the nonlinear models, but not at all by l.f.d.t. As in the previous data (5 September), the c.s.m. overpredicts spectral density in the high frequency (over 0.15 Hz) regions of the spectrum, while the d.s.m. exhibits a considerably smaller underprediction at high frequencies. Except for frequencies near the secondary peak, l.f.d.t. accurately predicts spectral shape. However, l.f.d.t. overpredicts the power at the spectral peak by 20% (compared with only a 5% overprediction by the d.s.m.). This leads credence to the hypothesis that the secondary peak is a result of nonlinear transfers of energy from the primary low frequency peak to its second harmonic.

Coherence spectra are shown in figure 11. The overall drop in coherence with increasing frequency and onshore distance agrees well with coherences predicted from the measured directional spectrum and equation (27), as was the case with the 5 September data set. The

PHILOSOPHICAL TRANSACTIONS OF THE ROYAL SOCIETY A MATHEMATICAL, PHYSICAL & ENGINEERING SCIENCES

nonlinear models do not differ significantly from each other, but they are substantially different from l.f.d.t. coherences at the secondary peak in the power spectrum. As the peak develops, the coherence between l.f.d.t. and the data becomes progressively lower. Conversely, the coherence at 0.127 Hz between the nonlinear models and the data is substantially higher on 11 September than it was for the 5 September data set (figure 6). The drop in coherence for l.f.d.t. is restricted to the same frequency band as is the secondary peak in the power spectrum;

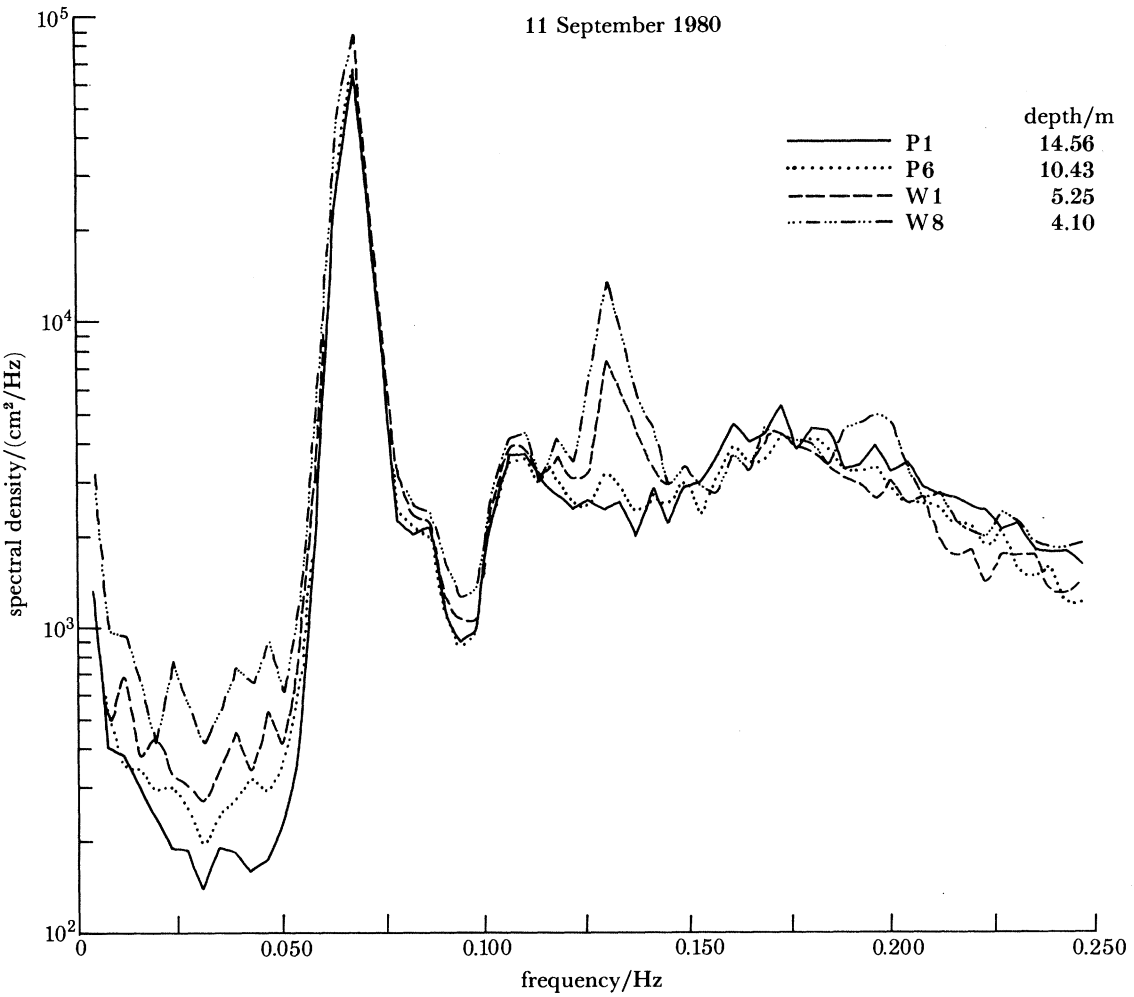

FIGURE 9. Measured power spectra of s.s.e. for the 11 September data set (similar to figure 4). Note the emergence of a secondary peak at the second harmonic of the primary.

at most frequencies higher and lower, there is no significant difference in coherence between linear and nonlinear models. However, examination of frequencies near 0.20 Hz at location W8 reveals a mild increase in coherence of the nonlinear models that is not present in the linear model. Although the deviation between nonlinear and linear model coherences is not significant at the 95% confidence level, the fact that it occurs at the third harmonic of the primary peak in the power spectrum is indicative of nonlinear transfers of energy to the third harmonic via near resonant interactions between the primary and secondary peaks.

At locations P8 and P11, in relatively deep water where little spectral evolution is observed

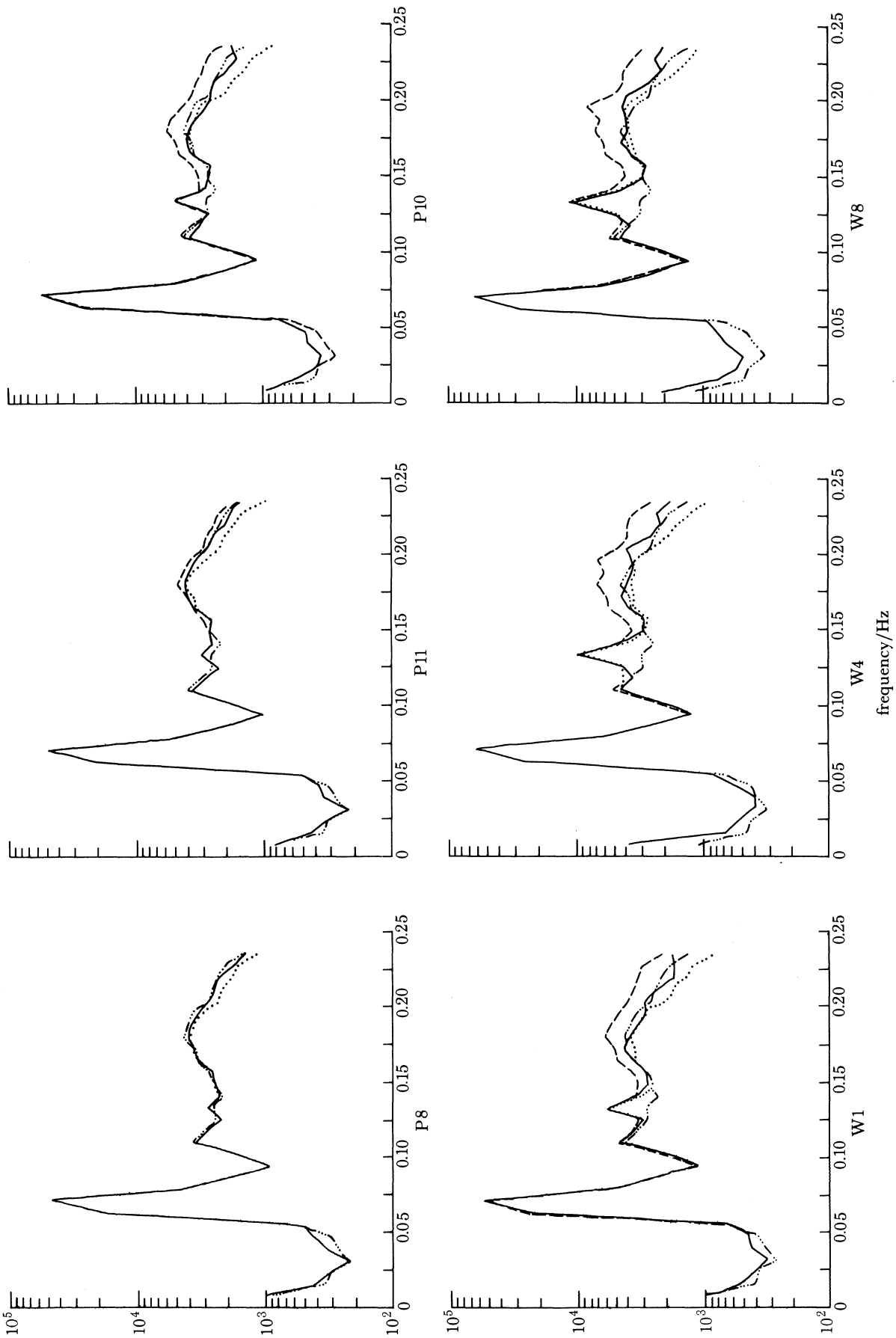

FIGURE 10. Comparison of predicted averaged power spectra of s.s.c. for the 11 September data set (——) (similar to figure 5). The nonlinear c.s.m. (– – –) and d.s.m. (· · ·) accurately predict the growth of the harmonic peak, while l.f.d.t. (—· · ·—) does not.

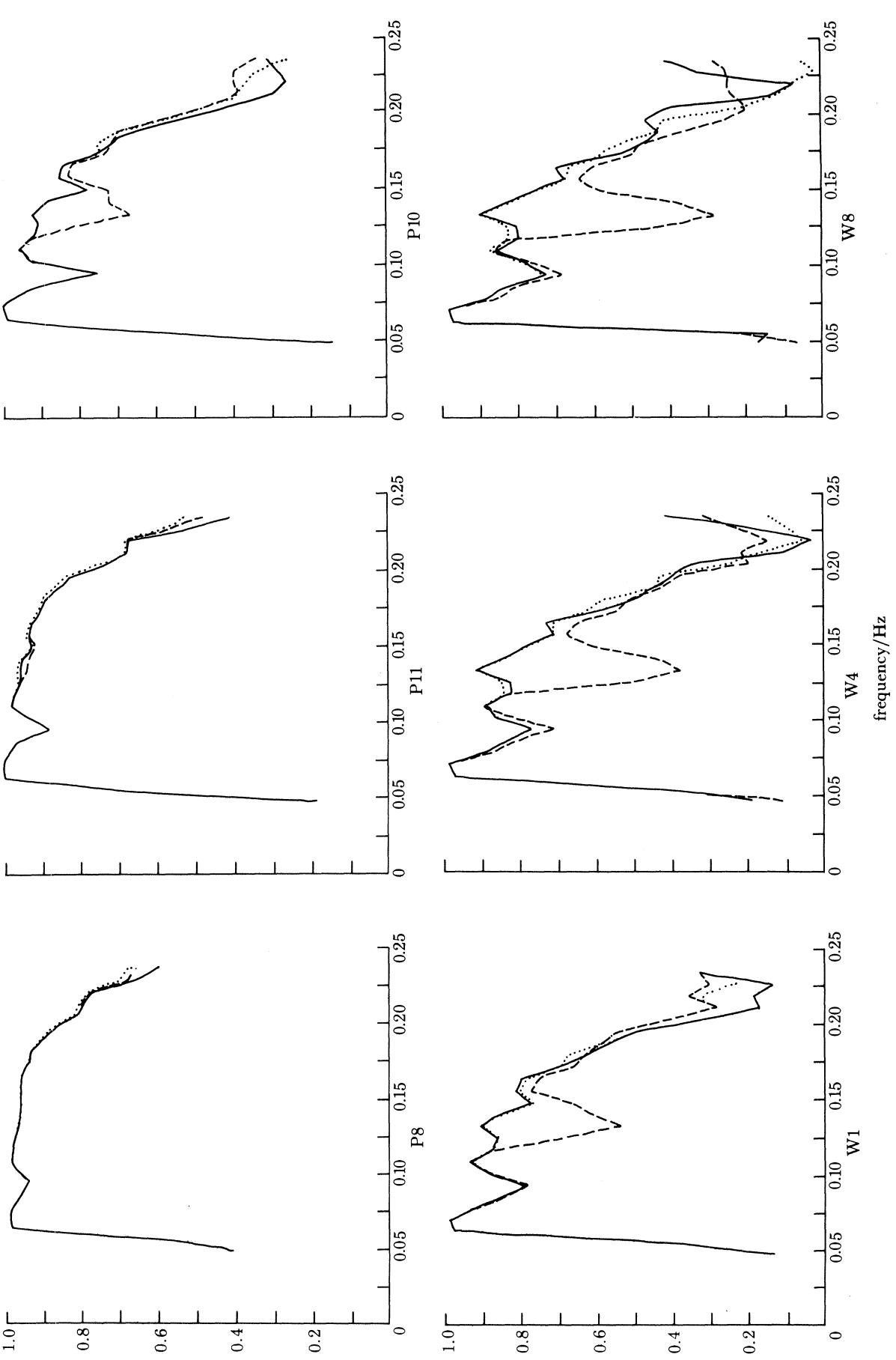

FIGURE 11. Smoothed coherence spectra for the 11 September data set (similar to figure 6). Flat-bottom, directional test coherences are not shown. L.f.d.t. predictions (– – –) have low coherence with the data in the frequency band corresponding to the secondary peak in the power spectrum, while the nonlinear models' predictions (c.s.m., · · ·; d.s.m., ——) have high coherence with the data in precisely this band.

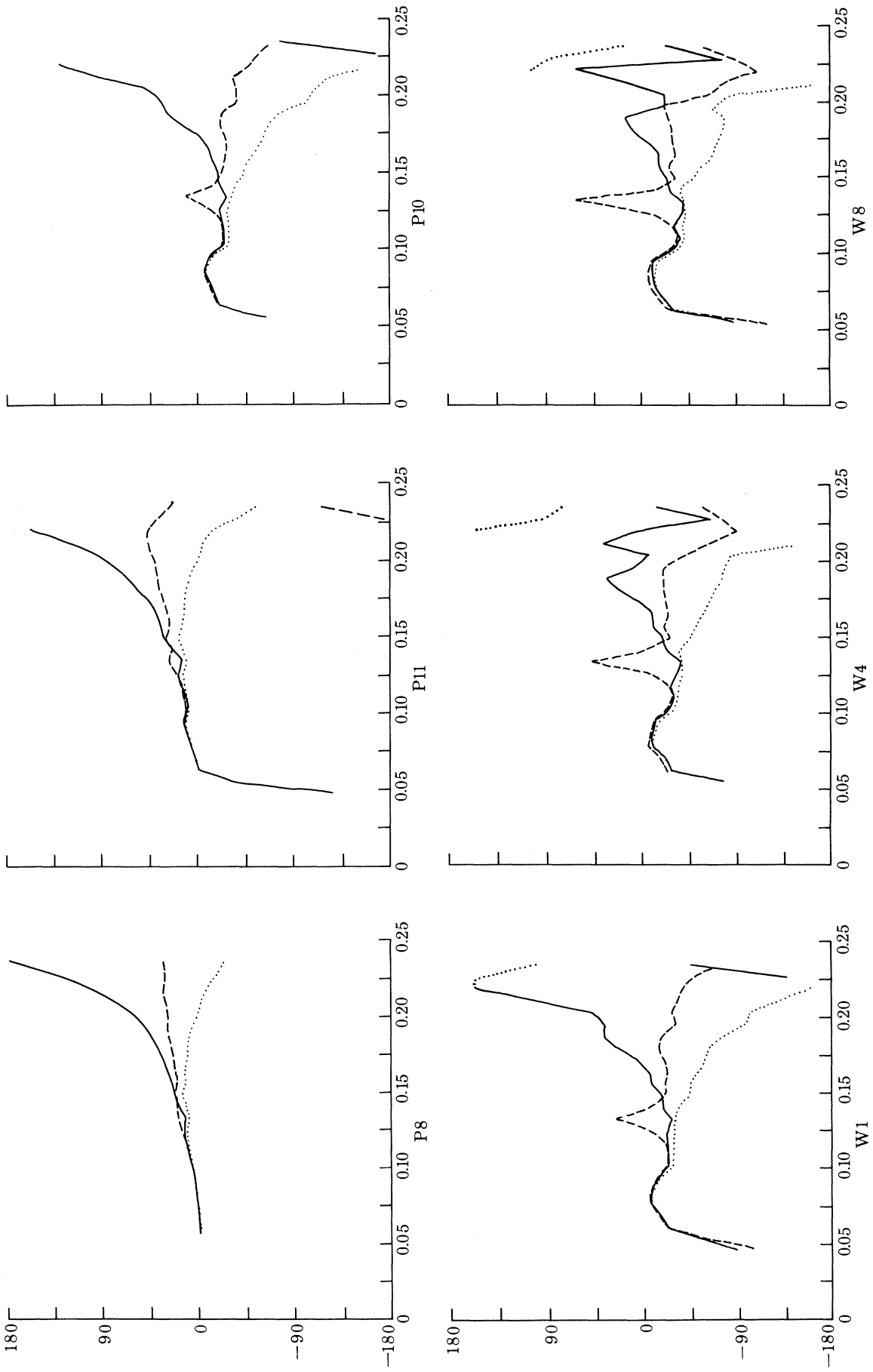

FIGURE 12. Spectra of phase between model predictions (d.s.m., ——; c.s.m., · · ·) and the data for the 11 September data set (similar to figure 7). L.f.d.t. (– – –) increasingly leads the data in the harmonic frequency band.

and coherences between all models and the data are high, the relative phase spectra between all models and the data (figure 12) are virtually identical with those of the 5 September data set (figure 7). As in the discussion for that set, phase deviations can be attributed to linear dispersion differences between the models. With the exceptions of the frequency band about 0.127 Hz for l.f.d.t. and the narrow band about 0.20 Hz for the d.s.m., relative phases between models and data are similar to those observed in the 5 September data set throughout the entire shoaling retion.

In the frequency band about 0.127 Hz, l.f.d.t. increasingly leads the data as depth decreases. It must be remembered that in this band, coherence between l.f.d.t. and the data is quite low; thus confidence intervals for phase increase, in this case to $\pm 35°$ at W8. Even so, the deviation is significant at all onshore locations. As no significant phase deviations between the nonlinear models and data are observed in this frequency band, it must be concluded that there is a nonlinearly induced phase change in addition to the observed power spectral transfer. The change is such that the phase speed of the second harmonic is greater than that of a free, linear wave with the same frequency.

A second difference between this data set and 5 September is apparent near 0.20 Hz for the d.s.m. at the most shoreward locations W4 and W8. Rather than a smoothly increasing phase difference between the model and the data, as would occur with waves obeying l.f.d.t. dynamics, the phase difference drops nearly to zero in this band. This frequency band is the third harmonic of the primary, and a slightly increased coherence between the d.s.m. and the data was observed as well. The phase results further confirm that nonlinear interactions, probably between the primary and the large second harmonic, are present in this band. Since the amplitude of the third harmonic is small, substantial phase modifications can take place (cf. (23*b*)), and thus the actual phase in the band can be coupled to the phase of the primary and second harmonic (which are predicted well by the nonlinear models), rather than by assuming the phase dictated by the linear dispersion relation.

(*c*) 9 *September*

The 9 September data set exhibits the most complicated evolution of any so far analysed. Composed of 17408 s of data obtained on a falling tide, the variance of s.s.e. at 10 m depth (measured to be 275 cm^2) falls between the low variance of 5 September and the high variance of 11 September. The power spectrum of s.s.e. is dominated by a broad peak centred at 0.09 Hz. The high frequency spectrum in depths greater than 10 m is flat and nearly 2 orders of magnitude down from the peak. Figure 13 shows data spectra through the shoaling region. As in the other data sets, there is no spectral evolution in depths greater than 10 m. However, through the shoaling region, the entire high frequency portion of the spectrum is amplified such that, in 4 m depth, spectral densities in the frequency band 0.15–0.21 Hz are 5–10 times greater than in 10 m depth.

As in the 11 September data set, the nonlinear models accurately predict spectral evolution throughout the shoaling region, while l.f.d.t. does not (figure 14). Although the c.s.m. appears to predict power spectral density more accurately than does the d.s.m. at frequencies greater than 0.17 Hz, the consistently large (20–40 %) overprediction of spectral density in the band 0.09–0.17 Hz makes the c.s.m. a less accurate predictor of overall spectral shape. Of some interest is the fact that the evolution of the spectrum begins with the emergence of a (non-significant at the 90 % level) peak at 0.19 Hz, the second harmonic of the most energetic

portion of the broad, low frequency spectral peak. The emergence of such a structure is not unexpected, as the peak–peak-harmonic triad interaction is expected to dominate early spectral evolution due to the larger amplitudes found at the peak of the power spectrum. The importance of off-peak interactions is clear, however, as in the shallower portions of the shoaling region the entire high frequency portion of the power spectrum has increased significantly.

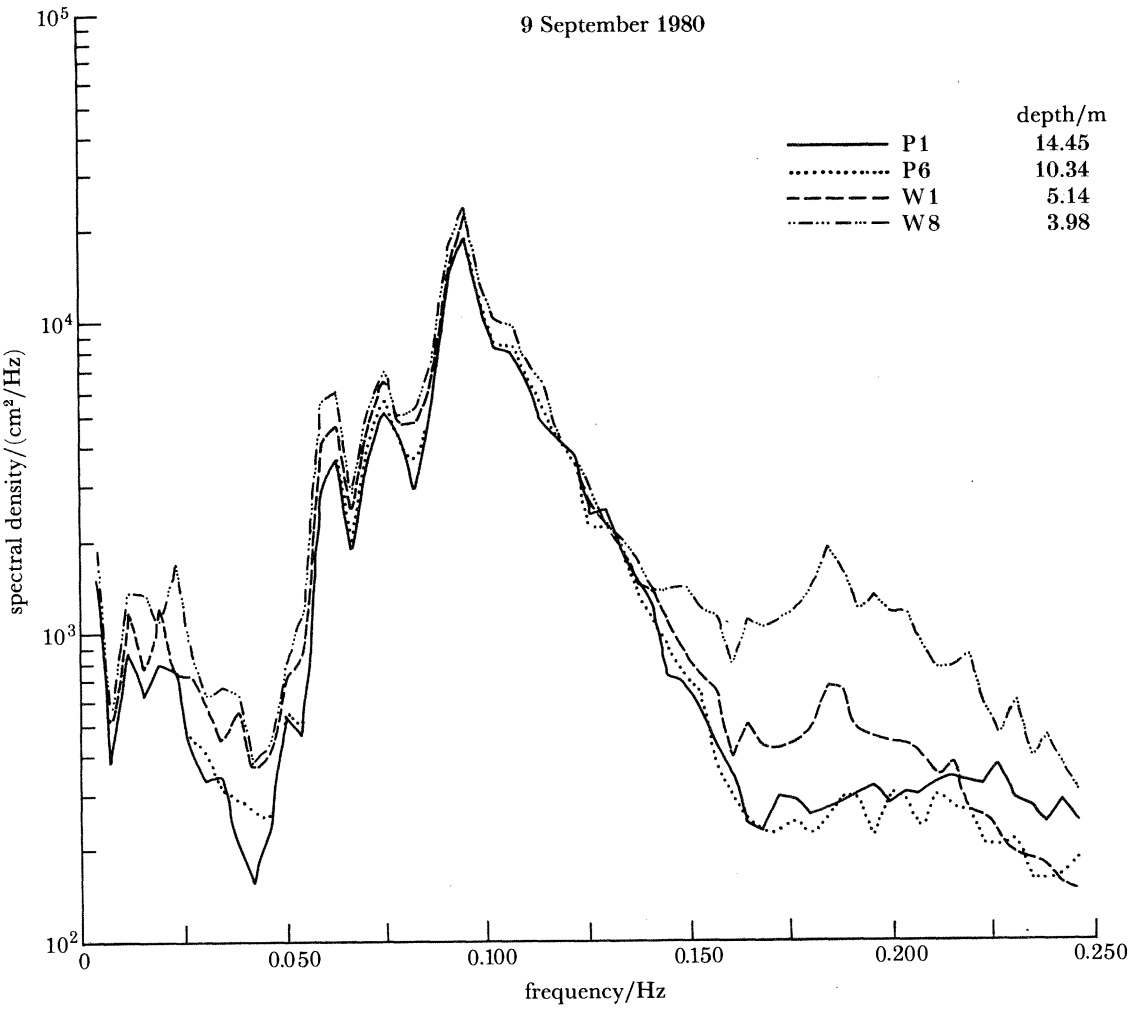

FIGURE 13. Measured power spectra of s.s.e. for the 9 September data set (similar to figure 4). The entire high frequency band (0.125–0.25 Hz) has greatly enhanced power in the shallow portions of the shoaling region.

The coherence spectra shown in figure 15 are further evidence of the complex evolution of the wave field as it propagates through the shoaling region. Apart from the barely significant coherence peak at 0.19 Hz apparent in the c.s.m. and d.s.m. spectra, the basic shapes of all model-data coherence spectra at locations P8 and P11 are again consistent with measured directional spectra. At all on–offshore locations, all models have high coherence with the data in the energetic frequency band 0.063–0.125 Hz. However, at shallow locations from P10 to W8, significant deviations between models are evident in the high frequencies. Coherence between l.f.d.t. and the data drops dramatically with decreasing depth, first in the band 0.13–0.20 Hz, then throughout the high frequencies. At the same time, coherences between

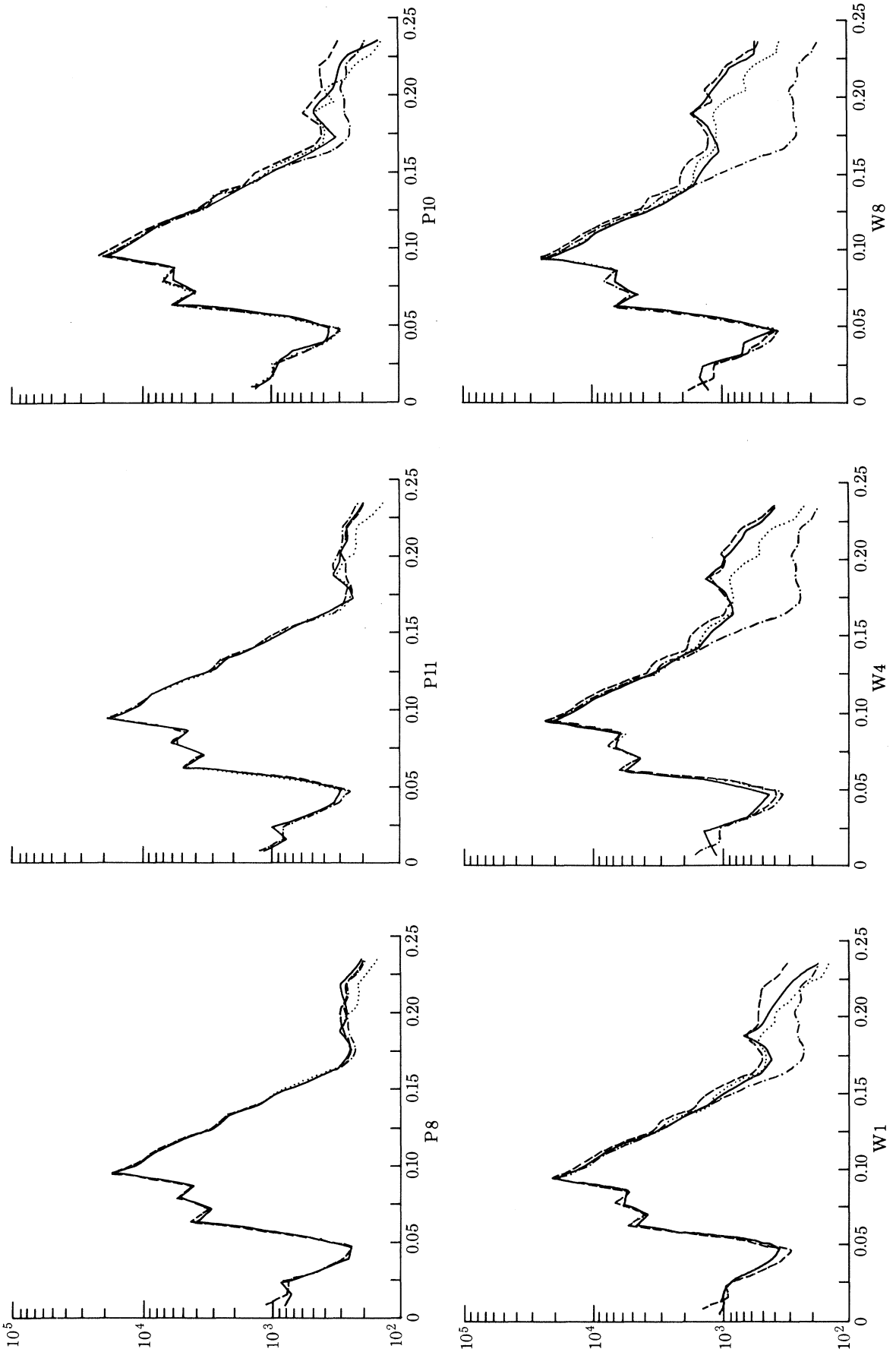

FIGURE 14. Comparison of predicted averaged power spectra for the 9 September data set (——) (similar to figure 5). The nonlinear models (d.s.m., · · ·; c.s.m., – – –) predict the enhancement of the high frequency power, while l.f.d.t. (—·—) does not.

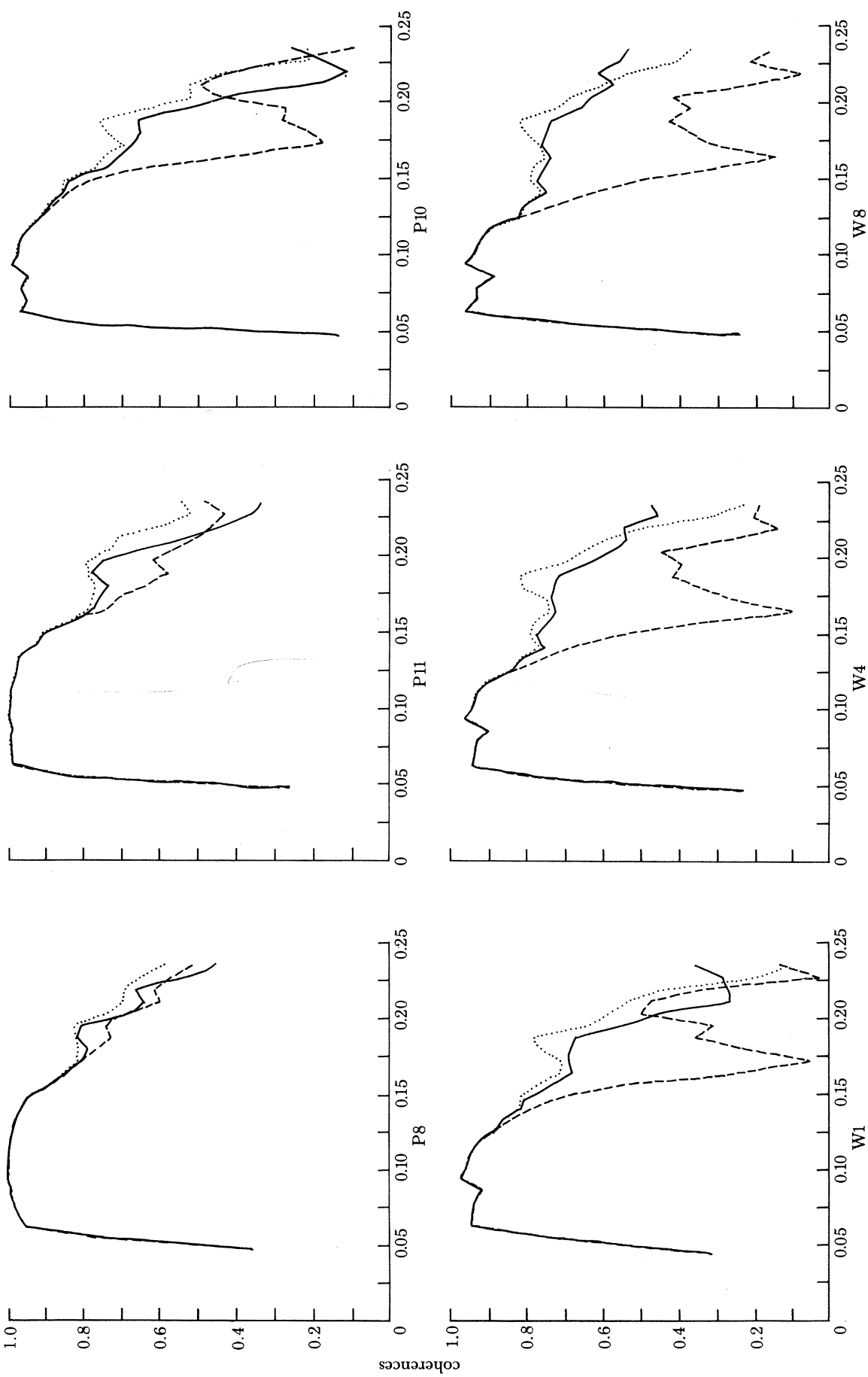

FIGURE 15. Smoothed coherence spectra for the 9 September data set (similar to figure 6). Flat-bottom, directional test coherences are not shown. The nonlinear models (d.s.m., ——; c.s.m., · · ·) have high coherence with the data at high frequencies, while l.f.d.t. (– – –) does not.

PHILOSOPHICAL TRANSACTIONS OF THE ROYAL SOCIETY A MATHEMATICAL, PHYSICAL & ENGINEERING SCIENCES

9 September 1980 (coincides)

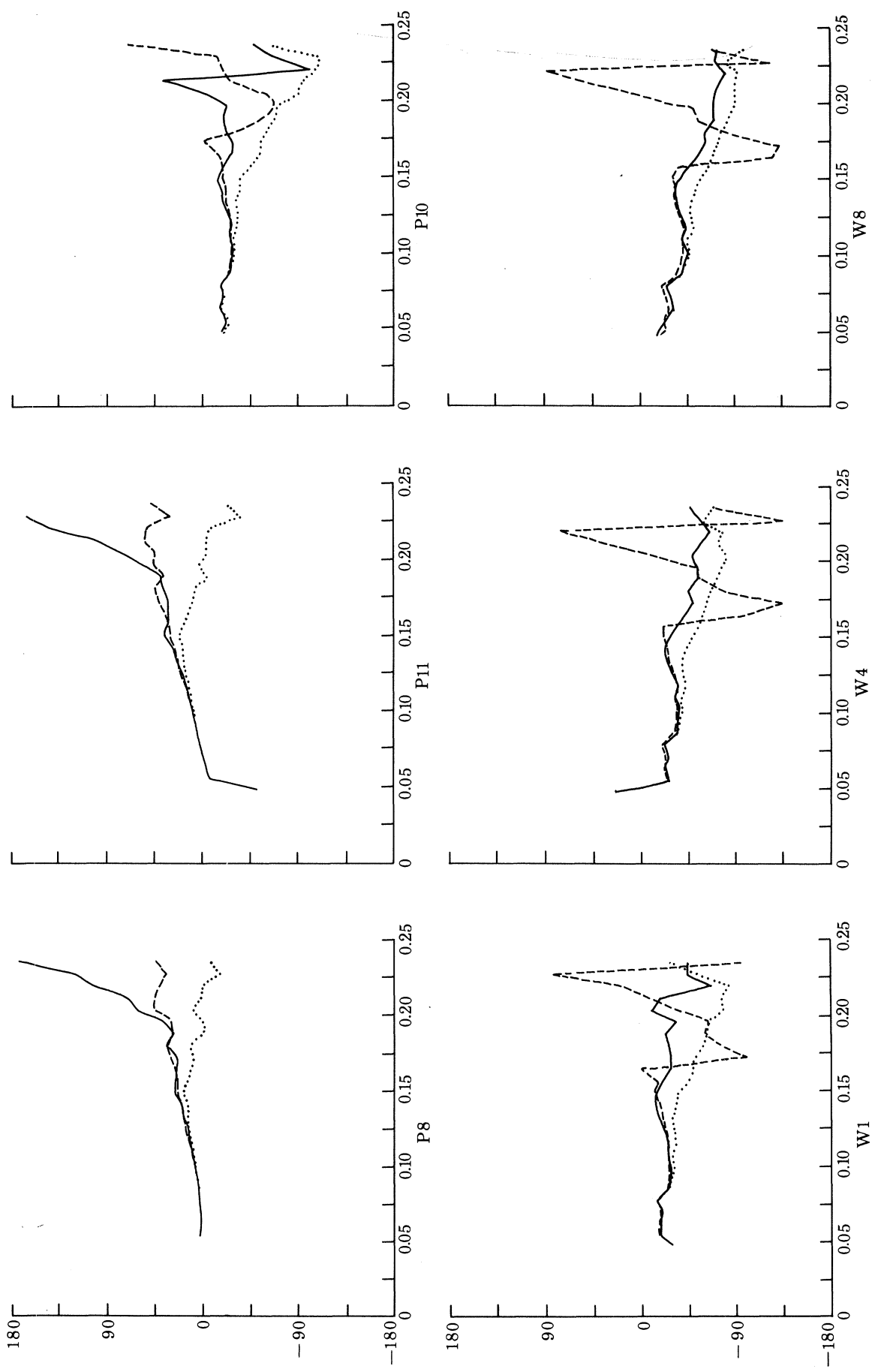

FIGURE 16. Spectra of phase between model predictions and the data for the 9 September data set (similar to figure 7): c.s.m., · · ·; d.s.m., ——; l.f.d.t., – – –.

the nonlinear models and the data actually increase significantly in the high frequency region. Such an effect clearly does not arise from finite directional spread in a homogeneous, linear wave field, but must be attributed to the fact that the high frequency wave field is dominated by nonlinear interactions with lower frequency components.

The nonlinearities are also evident in the phase spectra (figure 16). Phases at locations P8 and P11 evolve similarly to those of previous data sets, in accordance with simple l.f.d.t. dispersion. At the shallower locations from P10 to W8, the breakdown of linear dispersion is clear. The phase relation between linear theory and the data at high frequencies is neither consistent with zero phase lag, nor is it monotonic (although once again it must be remembered that the coherence between l.f.d.t. and the data is low in this region of frequency space). In terms of phase speeds, some frequency components appear to be travelling faster than predicted by l.f.d.t., and some slower! Rather than the d.s.m. leading the data in the high frequencies as predicted by linear dispersion arguments and observed in the basically 'linear' 5 September data set (figure 7), the model actually lags the data slightly. The c.s.m. phases exhibit none of the sharp lag predicted by linear dispersion, but are instead nearly identical with phases predicted by the d.s.m. It thus appears that nonlinear interactions, properly modelled by both the c.s.m. and the d.s.m., completely dominate the high frequency portion of the wave field in this particular data set.

5. Discussion and conclusions

The present work has developed and tested models that describe the changes undergone by wind generated surface waves (4–20 s periods) as a broad spectrum of such waves propagates shoreward over a shoaling bottom. Two one-dimensional models based on variants of the Boussinesq equations and incorporating the physics of multiple near resonant triads have been developed and implemented numerically. The models, which assume that all waves are normally incident to the beach, have no empirically determined parameters.

A field experiment that involved dense instrumentation of the shoaling region from 10 m to 3 m depth was successful in obtaining detailed measurements over a wide range of wave conditions. Three selected data sets spanning the range of observed wave conditions and spectral evolution have been analysed and compared with power spectra, coherence, and phase predictions of the two nonlinear shoaling models and linear, finite-depth theory.

Overall, both nonlinear models were good predictors of the power spectrum of sea–surface elevation throughout the shoaling region. Linear theory was considerably less accurate except under broad banded, low energy conditions. Coherences between predictions of all models and the data was uniformly high in the low frequency (generally energetic) region of the wind wave band. With the exception of those regions of space (both physical and frequency) where significant nonlinear evolution of the power spectrum was observed, the features of all model-data coherence spectra were similar and adequately accounted for by the measured directional spread of the wave field. Where nonlinear effects were important (shallow water, mid- to high-frequencies), coherences between the nonlinear models and the data improved markedly, while the coherences between l.f.d.t. and the data became dramatically lower. In spatial regions where nonlinear effects were small, l.f.d.t. was an accurate predictor of phase across the entire wind wave spectrum. In these regions, phase deviations between the nonlinear models and the data can be ascribed to differences in linear dispersion relations; the long wave

PHILOSOPHICAL TRANSACTIONS OF THE ROYAL SOCIETY A MATHEMATICAL, PHYSICAL & ENGINEERING SCIENCES

assumptions inherent in the derivation of the Boussinesq-type models make them poor predictors of wavenumber for high frequency waves in relatively deep water. Where nonlinear effects were important in the evolution of the power spectrum, the nonlinear models were good predictors of phase whereas l.f.d.t. was significantly poorer, indicating that nonlinear phase changes (which can, for instance, generate the observed asymmetrical shape of waves near breaking) are as evident as the more often-documented cross-spectral energy transfers.

The accurate predictions of the nonlinear shoaling models over a broad range of input wave conditions make them especially appealing. Some specific data sets (e.g. 5 September,

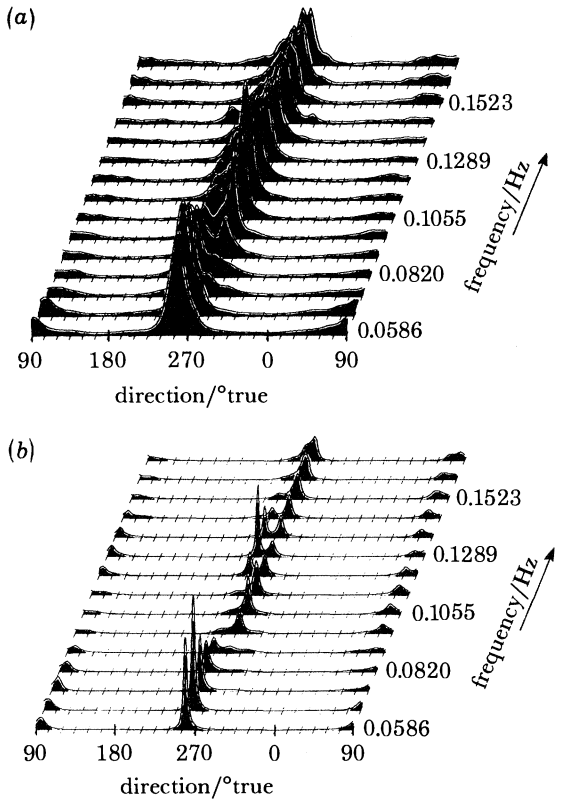

FIGURE 17. Frequency-directional spectra in the wind–wave band for the 11 September data set. The top spectrum (*a*) is obtained from m.l.e. analysis of the two-dimensional deep array shown in figure 2, excepting the nonfunctional current meter. The bottom spectrum (*b*) results from a similar analysis of the linear shallow array of wavestaffs W2–W7. Placement inaccuracies resulted in staffs W2 and W7 being far enough shoreward and seaward (respectively) of the longshore line to allow for the resolution of on-shore against offshore propagating energy. Scaling is such that at any frequency, the total area under the curve is proportional to the logarithm of spectral density in that band.

figures 4–7) are predicted well by l.f.d.t. The evolution of harmonics in some data sets (11 September, figures 9–12) is reminiscent of Stokes-type forced theories (although the similarity is merely illusory, as the Ursell number in 5 m depth for this data set is over 1). In all cases so far observed, the more general c.s.m. and d.s.m. accurately predict the observed spectral evolution of the wave field through the shoaling region; in the three data sets analysed here in detail, the models properly predict nonlinear phase evolution as well.

Directional effects appear to play little role in the nonlinear evolution of the data sets analysed here. In part this is due to the fact that Torrey Pines Beach has few open windows

to the deep ocean, and thus energetic low and mid-frequency waves tend to have narrow, well defined, nearly normally incident directional spectra. More generally, however, these waves refract considerably before entering the relatively shallow water of the shoaling region, and thus the extremely broad directional distributions typical of the open ocean are not expected.

Figure 17 shows two, averaged, frequency-directional spectra from the 11 September data set. The top figure displays data obtained from the two-dimensional array in 10 m depth (see figure 2). Note that the energy in the low frequency peak of the power spectrum (0.066 Hz) is directed from approximately 15° south of true west, and has a width of only 25°. It is likely that this swell is being generated by a distant storm in the southern hemisphere. Pawka (1982) discusses details of the directional spectrum for similar data sets. Of interest to the present study is the fact that, although the majority of the energy at frequencies greater than 0.10 Hz is directed from the northern quadrant, approximately half of the energy at the harmonic frequency (0.127 Hz) is directed from the south, colinear with the low frequency primary. The effect is enhanced in the data from the shallow array, shown in the lower half of figure 17. In general, directional spreads measured at the shallow array are narrower than those measured at the deep array, as expected on the basis of simple linear refraction. In the harmonic frequency band (0.12–0.13 Hz), the vast majority of the energy comes not from the north but from the south, in contrast to neighbouring bands. This is expected if, as hypothesized in §4, the energy in the harmonic peak is due primarily to nonlinear transfers via peak–peak-harmonic triad interactions. As the resonance conditions (8*b*) or (22*b*) are vector equations, any peak–peak-harmonic interaction will force harmonic waves whose wavenumbers point in the direction of the peak waves.

The directional spectra also provide preliminary bounds on the amount of seaward-propagating energy in the shoaling region. Direct integration of directional spectral estimates in the frequency range 0.059–0.152 Hz for all 11 data sets reveals that at no time is more than 25% of the total energy in any band propagating seaward in the window 45–135° at the shallow array, while less than 20% of the total energy is found to propagate seaward at the deep array. Average values of seaward-propagating energy are 17% for the shallow array and 14% for the deep array. However, model testing of the m.l.e. indicated that the data-adaptive analysis technique, when applied to the arrays used in this experiment, windowed incoming energy incorrectly into outgoing directions. The model tests suggest that there is a strong possibility that the true amount of seaward-propagating energy is less than 10% of the total energy at frequencies in the wind wave band. Such small 'reflection' is not inconsistent with the qualitative conclusions drawn by Peregrine (1967) based on the linear analysis of Kajiura (1961). Inclusion of seaward-propagating energy in the nonlinear models is a formidable task; however, predictions of the one-dimensional models clearly are not significantly affected by such small amounts of outgoing energy. Should a more quantitative description of seaward-propagating energy be desired, a special purpose analysis technique with minimal windowing error of incoming to outgoing energy, similar to those discussed in Davis & Regier (1977) and Pawka (1982), should be implemented.

The sloping bottom was found to play only a minor role in determining the spectral evolution of the wave field through the shoaling region. In the course of preliminary model testing, examples of many spectral shapes were numerically propagated in water of constant, 5 m depth typical of the shoaling region. Many qualitative features of the spectral evolution, such as harmonic generation from initially narrow-banded spectra, or the pronounced enhancement

of the entire high frequency band for initially broader-banded spectra, were similar to those actually observed in the data from a mildly sloping beach. Bottom slope appears explicitly only in the linear shoaling terms in the nonlinear models, and implicitly in the calculation of total phase necessary to determine the trigonometric modulation of the nonlinear coupling.

Differences between the linear shoaling terms, due to differences between linear dispersion relations, account for much of the deviation between power spectral predictions of the nonlinear models and the data. This is true at all frequencies in the 5 September data set and at those (generally high) frequencies in other data sets where nonlinear spectral evolution is not apparent. Simmons (1969) and McGoldrick (1965) show that lowest order energy flux is conserved for a single resonant triad. The physical arguments of Simmons (1969) hold for our system which contains multiple resonances. The non-dispersive form of the dispersion relation (14*b*) overpredicts (in comparison to l.f.d.t.) the increase in modal energy (proportional to the square of the mode amplitude) with decreasing depth necessary to conserve lowest order energy flux over most of the wind wave band. Conversely, the dispersion relation (28*b*) underpredicts the increase, but remains within 10% of the value predicted by l.f.d.t. for frequencies less than 0.17 Hz everywhere in the shoaling region. (Care must be taken when attempting to isolate the effects of individual terms in the rate equations. Since the c.s.m. and d.s.m. allow weak nonlinear interactions across all frequencies, a misprediction in the evolution equations, even if confined initially to a small band of frequencies, can feed back through the nonlinear coupling to cause errors at other frequencies and other on–offshore locations.)

The observed lack of power spectral evolution between 14 m depth (P1) and 10 m depth (P6) strongly indicates that the process of triad near resonance modelled by the c.s.m. and the d.s.m. is significant only in the relatively shallow shoaling region. Although the models are not valid in depths much greater than 10 m due to the breakdown of the long wave assumptions over much of the wind wave frequency band, the trend toward increasing inability to satisfy the interaction conditions for triads containing high frequency waves suggests that the nonlinear triad mechanism is unimportant in such relatively large depths. This bodes well for future attempts to smoothly match the present model with one more appropriate to deep water.

The authors wish to thank the staff and students of the Center for Coastal Studies for their invaluable efforts during the field experiment. Special thanks are due to D. L. Inman, R. L. Lowe, P. M. Cunningham, P. d'Acri and D. McLean. This research was supported by the Office of Naval Research Code 422CS (Coastal Studies), contract no. N00014-75-C-0300. Financial support for M.H.F. was provided by a Sea Grant Traineeship, project no. R/CZ-N-4D. The manuscript was written while one of us (M.H.F.) had an appointment at the Marine Sciences Research Center of the State University of New York at Stony Brook. Revision of the manuscript was carried out at the Jet Propulsion Laboratory, California Institute of Technology under contract with the National Aeronautics and Space Administration.

References

Airy, G. B. 1845 Tides and waves. In *Encyclopedia metropolitana*, p. 289, art. 192. London.

Armstrong, J. A., Bloembergen, N., Ducuing, J. & Pershan, P. S. 1962 Interactions between light waves in a nonlinear dielectric. *Phys. Rev.* B **127**, 1918–1939.

Aubrey, D. G. 1978 Statistical and dynamical prediction of changes in natural sand beaches. Ph.D. thesis, University of California, San Diego. (194 pp.)

Barber, N. F. 1961 The directional resolving power of an array of wave detectors. In *Ocean wave spectra*, pp. 137–150. New Jersey: Prentice-Hall.

PHILOSOPHICAL TRANSACTIONS OF THE ROYAL SOCIETY A MATHEMATICAL, PHYSICAL & ENGINEERING SCIENCES

Benney, D. J. & Saffman, P. G. 1966 Nonlinear interactions of random waves in a dispersive medium. *Proc. R. Soc. Lond.* A **289**, 301–320.
Boussinesq, J. 1871 Théorie générale des mouvements qui sont propagés dans un canal rectangulaire horizontal. *C. r. hebd. Séanc, Acad. Sci., Paris* **73**, 256–260.
Bretherton, F. P. 1964 Resonant interactions between waves: the case of discrete oscillations. *J. Fluid Mech.* **20**, 457–480.
Bryant, P. J. 1973 Periodic waves in shallow water. *J. Fluid Mech.* **59**, 625–644.
Bulirsch, R. & Stoer, J. 1966 Numerical treatment of ordinary differential equations by extrapolation methods. *Numerische Math.* **8**, 1–13.
Carrier, G. F. & Greenspan, H. P. 1958 Water waves of finite amplitude on a sloping beach. *J. Fluid Mech.* **4**, 97–109.
Cartwright, D. E. 1962 Analysis and statistics. In *The sea* (ed. M. N. Hill), vol. 1, pp. 567–586. New York: Interscience.
Chu, V. H. & Mei, C. C. 1970 On slowly-varying Stokes waves. *J. Fluid Mech.* **41**, 873–887.
Cole, J. D. 1968 *Perturbation methods in applied mathematics.* Massachusetts: Blaisdell. (260 pp.)
Cunningham, P. M., Guza, R. T. & Lowe, R. L. 1979 Dynamic calibration of electromagnetic flow meters. *I.E.E.E. Trans.* Oceans **79**, 298–301.
Davis, R. E. & Regier, L. A. 1977 Methods for estimating directional spectra from multi-element arrays. *J. mar. Res.* **35**, 453–477.
Flick, R. E., Guza, R. T. & Inman, D. L. 1981 Elevation and velocity measurements of laboratory shoaling waves. *J. geophys. Res.* **86**, 4149–4160.
Flick, R. E., Lowe, R. L., Freilich, M. H. & Boylls, J. C. 1979 Coastal and laboratory wavestaff system. *I.E.E.E. Trans.* Oceans **79**, 623–625.
Friederichs, K. O. 1948 Water waves on a shallow sloping beach. *Communs pure appl. Math.* **1**, 109–134.
Gable, C. G. 1979 Report on data from the nearshore sediment transport study at Torrey Pines, California Institute of Marine Resources ref. no. 79–8, La Jolla.
Gragg, W. B. 1963 Repeated extrapolation to the limit in the numerical solution of ordinary differential equations. Ph.D. thesis, University of California, Los Angeles (103 pp.)
Grimshaw, R. 1970 The solitary wave in water of variable depth. *J. Fluid Mech.* **42**, 639–656.
Guza, R. T. & Thornton, E. B. 1980 Local and shoaled comparisons of sea–surface elevations, pressures, and velocities. *J. geophys. Res.* **85**, 1524–1530.
Hanson, E. T. 1926 The theory of ship waves. *Proc. R. Soc. Lond.* A **111**, 491–529.
Hasselmann, K. 1962 On the nonlinear energy transfer in a gravity wave spectrum I. *J. Fluid Mech.* **12**, 481–500.
Hasselmann, K. 1963 On the nonlinear energy transfer in a gravity wave spectrum II. *J. Fluid Mech.* **15**, 273–281.
Hasselmann, K. 1966 Feynman diagrams and interaction rules of wave–wave scattering processes. *Rev. Geophys. Space Phys.* **4**, 1–32.
Haubrich, R. A. 1965 Earth noise, 5 to 500 millicycles per second. *J. geophys. Res.* **70**, 1415–1427.
Herterich, K. & Hasselmann, K. 1980 A similarity relation for the nonlinear energy transfer in a finite-depth gravity-wave spectrum. *J. Fluid Mech.* **97**, 215–224.
Holloway, G. 1980 Oceanic internal waves are not weak waves. *J. phys. Oceanogr.* **10**, 906–914.
Inman, D. L., Zampol, J. A., White, T. E., Hanes, D. M., Waldorf, B. W. & Kastens, K. A. 1980 Field measurements of sand motion in the surf zone. *Proc. 17th Coastal Eng. Conf.* vol. 2, pp. 1215–1234. New York: A.S.C.E.
James, I. D. 1974 Nonlinear waves in the nearshore region: shoaling and setup. *Estuar. coast. mar. Sci.* **2**, 207–234.
Jenkins, G. M. & Watts, D. G. 1968 *Spectral analysis and its applications.* San Francisco: Holden-Day. (525 pp.)
Johnson, R. S. 1973 On the development of a solitary wave moving over an uneven bottom. *Proc. Camb. phil. Soc.* **73**, 183–203.
Kajiura, K. 1961 On the partial reflection of water waves passing over a bottom of variable depth. *Inter. Union of Geodesy and Geophys.* Monograph no. 24. *Tsunami Symposia*, pp. 206–230.
Keller, J. B. 1948 The solitary wave and periodic waves in shallow water. *Communs pure appl. Math.* **1**, 323–339.
Korteweg, D. J. & deVries, G. 1895 On the change in form of long waves advancing in a rectangular channel, and on a new type of long stationary waves. *Phil. Mag.* **39**, 442–443.
Lavelle, J. W., Yound, R. A., Swift, D. J. & Clarke, T. L. 1978 Near-bottom sediment concentration and fluid velocity measurements on the inner continental shelf, New York. *J. geophys. Res.* **83**, 6052–6062.
LeMahaute, B. & Webb, L. M. 1964 Periodic gravity waves over a gentle slope at a third order of approximation. *Proc. 9th Coastal Eng. Conf.* pp. 23–40. New York: A.S.C.E.
Longuet-Higgins, M. S. 1976 On the nonlinear transfer of energy in the peak of a gravity wave spectrum: a simplified model. *Proc. R. Soc. Lond.* A **347**, 311–328.
Lowe, R. L., Inman, D. L. & Brush, B. M. 1972 Simultaneous data system for instrumenting the shelf. *Proc. 13th Coastal Eng. Conf.* pp. 95–112. New York: A.S.C.E.
McGoldrick, L. F. 1965 Resonant interactions among capillary-gravity waves. *J. Fluid Mech.* **21**, 305–331.
Mei, C. C. & LeMehaute, B. 1966 Note on the equations of long waves over an uneven bottom. *J. Geophys. Res.* **71**, p. 393–400.

PHILOSOPHICAL TRANSACTIONS OF THE ROYAL SOCIETY A MATHEMATICAL, PHYSICAL & ENGINEERING SCIENCES

Mei, C. C. & Unluata, U. 1972 Harmonic generation in shallow water waves. In *Waves on beaches and resulting sediment transport* (ed. R. E. Meyer), pp. 181–202. New York: Academic Press.
Miles, J. W. 1980 Solitary waves. *A. Rev. Fluid Mech.* **12**, 22–43.
Minorsky, N. 1974 *Nonlinear oscillations*. Huntington: Krieger. (714 pp.)
Nayfeh, A. H. 1981 A comparison of perturbation methods for nonlinear hyperbolic waves. In *Singular perturbations and asymptotics* (ed. R. E. Meyer & S. Parter), pp. 223–276. New York: Academic Press.
Newell, A. C. 1968 The closure problem in a system of random gravity waves. *Rev. Geophys.* **6**, 1–31.
Ostrovskiy, L. A. & Pelinovskiy, E. L. 1970 Wave transformation on the surface of a fluid of variable depth. *Izv. Atmos. Ocean. Phys.* **6**, 552–555.
Pawka, S. S. 1982 Wave directional characteristics on a partially sheltered coast. Ph.D. thesis, University of California, San Diego. (246 pp.)
Pawka, S. S., Inman, D. L., Lowe, R. L. & Holmes, L. 1976 Wave climate at Torrey Pines Beach, California. Tech. paper 76-5, Coastal Engng Res. Center, Fort Belvoir. (372 pp.)
Peregrine, D. H. 1967 Long waves on a beach. *J. Fluid Mech.* **27**, 815–827.
Peregrine, D. H. 1972 Equations for water waves and the approximations behind them. In *Waves on beaches and resulting sediment transport* (ed. R. E. Meyer), pp. 95–122. New York: Academic Press.
Phillips, O. M. 1960 On the dynamics of unsteady gravity waves of finite amplitude, the elementary interactions. *J. Fluid Mech.* **9**, 193–217.
Phillips, O. M. 1977 *The dynamics of the upper ocean*, 2nd edn. Cambridge University Press. (336 pp.)
Rayleigh, Lord 1911 Hydrodynamical notes. *Phil. Mag.* **21**, 177–195.
Simmons, W. F. 1969 A variational method for weak resonant wave interactions. *Proc. R. Soc. Lond.* A **309**, 551–575.
Skjelbreia, L. & Hendrickson, J. 1960 Fifth order gravity wave theory. *Proc. 7th Coastal. Eng. Conf.*, p. 184–196. New York: A.S.C.E.
Stiassnie, M. & Peregrine, D. H. 1980 Shoaling of finite-amplitude surface waves on water of slowly-varying depth. *J. Fluid Mech.* **97**, 783–805.
Stoer, J. 1972 Extrapolation methods for the solution of initial value problems and their practical realization. In *Lecture notes in mathematics*, **362** (ed. A. Dold & B. Ekman). Berlin: Springer-Verlag.
Stoker, J. J. 1957 *Water waves*. New York: Interscience. (567 pp.)
Stokes, G. G. 1847 On the theory of oscillatory waves. *Trans. Camb. phil. Soc.* **8**, 441–455.
Svendsen, Ib. A. & Hansen, J. B. 1978 On the deformation of periodic long waves over a gently sloping bottom. *J. Fluid Mech.* **87**, 433–448.
Ursell, F. 1953 The long-wave paradox in the theory of gravity waves. *Proc. Camb. phil. Soc.* **49**, 685–694.
Whitham, G. B. 1974 *Linear and nonlinear waves*. New York: Wiley. (636 pp.)
Whitham, G. B. 1979 *Lectures on wave propagation*. Bombay: Tata Institute of Fundamental Research (148 pp.)
Willebrand, J. 1975 Energy transport in a nonlinear and inhomogeneous random gravity wave field. *J. Fluid Mech.* **70**, 113–126.

PHILOSOPHICAL TRANSACTIONS OF THE ROYAL SOCIETY A MATHEMATICAL, PHYSICAL & ENGINEERING SCIENCES